Journal of Computational Physics 378 (2019) 615–633

Contents lists available at ScienceDirect

Journal of Computational Physics

www.elsevier.com/locate/jcp

Inclusion of no-slip boundary conditions in the MEEVC scheme

G.G. de Diego [a,*], A. Palha [b], M. Gerritsma [b]

[a] Fakultät für Mathematik, Universität Duisburg-Essen, Germany
[b] Delft University of Technology, Faculty of Aerospace Engineering, Netherlands

ARTICLE INFO

Article history:
Received 20 December 2017
Received in revised form 3 October 2018
Accepted 14 November 2018
Available online 20 November 2018

Keywords:
Navier–Stokes
Mimetic discretization
Velocity boundary conditions
MEEVC scheme

ABSTRACT

This work presents three methods for enforcing tangential velocity boundary conditions for the MEEVC scheme, which was shown to be mass, enstrophy, energy and vorticity conserving scheme in the case of inviscid flow [1]. While the normal velocity component can be strongly imposed in a div-conforming formulation for the velocity field, inclusion of the tangential velocity needs to be set through an appropriate choice of vorticity boundary conditions. Three methods to impose the tangential velocity boundary condition will be discussed: The kinematic Dirichlet formulation, the kinematic Neumann formulation and the dynamic Neumann formulation. The conservation properties of each of the resulting schemes are analyzed and numerical results are shown for the Taylor–Green vortex and for the dipole collision test cases. These confirm that kinematic Neumann vorticity boundary conditions perform best.

© 2018 Elsevier Inc. All rights reserved.

1. Introduction

1.1. Structure-preserving methods

Physics-compatible (or structure-preserving) methods can be defined as numerical methods that aim to preserve a set of qualitative and global features of a differential equation at the discrete level, such as conservation laws or symmetries. In contrast to the more traditional approach in numerical analysis, in which a scheme is constructed with the sole objective of keeping local truncation errors as low as possible, the discrete dynamical system resulting from a physics-compatible method can have the same properties as its continuous counterpart, [2,3] and [4].

For the specific case of the incompressible Navier–Stokes equations, the physics of the system is described in terms of conservation of mass and linear momentum. The fidelity of a numerical solver will depend on its capability to represent conservation laws correctly. For example, turbulent flow computations require an accurate reproduction of the energy cascade and, to this end, conservation of kinetic energy in the inviscid limit is fundamental, for both DNS [5] and LES [6] simulations.

Mimetic methods can be considered a particular subclass of physics-compatible methods which describe the continuous and discrete differential models in terms of differential geometry and algebraic topology, respectively [7,8]. The use of differential forms for describing the field variables distinguishes quantities associated to points, lines, surfaces and volumes,

* Corresponding author.
E-mail address: gonzalogddiego@gmail.com (G.G. de Diego).

https://doi.org/10.1016/j.jcp.2018.11.025
0021-9991/© 2018 Elsevier Inc. All rights reserved.

recognizing that these should be treated in a fundamentally different manner when discretized. These geometrical aspects are encoded in differential complexes, such as the de Rham complex [7–10].

1.2. The MEEVC scheme

This work is the continuation of a previous publication in which a mass, energy, enstrophy and vorticity conserving (MEEVC) mimetic spectral element method for the 2D incompressible Navier–Stokes equations was presented [1]. These conservation properties are possible due to the use of a $(\vec{u}, p, \omega)$-formulation of the Navier–Stokes equations in the rotational form, a combination of finite element spaces that satisfy the divergence-free nature of the velocity field and an energy-preserving time integrator.

When considering boundary conditions for the MEEVC scheme, prescribing the tangential velocity along the boundary $\partial\Omega$ of a domain Ω is not straightforward. The velocity vector $\vec{u}$ is sought in the function space $H(\mathrm{div}, \Omega)$, the space of square-integrable vector fields whose divergence is square-integrable. When considering a finite element approximation of $H(\mathrm{div}, \Omega)$, square integrability of the divergence field translates into continuity of the normal components of the discrete velocity $\vec{u}_h$ along the interfaces of the elements [11].

As a consequence, the degrees of freedom of finite element subspaces of $H(\mathrm{div}, \Omega)$ are associated to the *fluxes* of $\vec{u}$ through the faces of the elements, without ensuring continuity of the tangential components of $\vec{u}$ across the elements. Therefore, strong prescription of tangential boundary conditions is not possible and, as will be shown here, tangential velocity boundary conditions must be imposed weakly by means of vorticity boundary conditions. This difficulty was avoided in the first paper [1] by considering flow problems with periodic boundary conditions.

1.3. Prescription of vorticity boundary conditions

The problem of vorticity boundary conditions arises in many different numerical solvers and remains a long-standing problem in computational fluid dynamics. Many different possibilities have been investigated over the past decades, although no consensus has been reached as to whether vorticity boundary conditions should be of Dirichlet or Neumann type, if they should be local or global (integral) or if they should be related to the more natural velocity boundary conditions by means of kinematic or dynamic relations [12–14].

From a historical point of view, Lighthill's analysis of vorticity creation along solid walls [15] set the standard for different vorticity schemes: tangential velocity boundary conditions are intimately related to the strength of a thin vortex sheet generated along the solid surface. The strength of these vortex sheets can be calculated as a correction to the slip velocity which results from a potential flow solution (see Chorin [16] and J.C. Wu [17] for implementations). An important point raised by Lighthill and treated in various theoretical analyses [18,19] is the relationship between vorticity generation and the tangential pressure gradient along a solid wall. J.Z. Wu et al. [20] implement vorticity boundary conditions following this line of reasoning and come to the conclusion that vorticity generation along the boundary must be calculated as a flux.

More in line with the current work, the problem of imposing vorticity boundary conditions arises when considering finite element solvers for the Navier–Stokes equations in a velocity–vorticity form. Unlike the work presented in this manuscript, most solvers presented in literature use Taylor–Hood elements [21] and seek the velocity field in a subset of $\left(H^1(\Omega)\right)^n$, with $n = 2$ or 3; as a consequence both the normal and the tangential velocity components can be prescribed strongly but mass conservation cannot be satisfied exactly. Use of the vorticity transport equation requires the prescription of Dirichlet [22–26] or Neumann vorticity boundary conditions [27,28]. Furthermore, an alternative that can be found in literature is the weak prescription of the kinematic definition of ω by means of a penalty method [29].

2. Formulation of the problem

In this section, the weak formulation of the 2D incompressible Navier–Stokes equations is constructed following [1] and the problem of prescribing tangential boundary conditions is addressed. It is shown that the boundary conditions for the vorticity transport equation must be related to the tangential velocity along the boundary. Finally, three different methods are presented that enable the prescription of tangential velocity boundary conditions by means of vorticity boundary conditions.

2.1. Formulation of the Navier–Stokes equations

Two-dimensional viscous incompressible flows are modeled by the Navier–Stokes equations, defined on a domain $\Omega \subset \mathbb{R}^2$. These equations are generally expressed in the so-called primitive form, based on the equations for conservation of momentum and of mass, and solved for the flow velocity $\vec{u} : \Omega \times (0, t_F] \to \mathbb{R}^2$ and pressure $p : \Omega \times (0, t_F] \to \mathbb{R}$:

$$\begin{cases} \dfrac{\partial \vec{u}}{\partial t} + (\vec{u} \cdot \nabla)\vec{u} + \nabla p = \nu \Delta \vec{u} & \text{in } \Omega \times (0, t_F], \\ \nabla \cdot \vec{u} = 0 & \text{in } \Omega \times (0, t_F], \end{cases} \tag{1}$$

where $t_F > 0$, ν is the kinematic viscosity coefficient and Δ is the Laplace operator. In this work, the following velocity boundary conditions will be considered:

$$\vec{u}\cdot\vec{n} = k(\boldsymbol{x},t), \quad \vec{u}\times\vec{n} = g(\boldsymbol{x},t), \quad \text{on } \partial\Omega\times(0,t_F], \tag{2}$$

with $\vec{n}$ the outward normal vector defined along the boundary of the domain $\partial\Omega$ and $g:\partial\Omega\times\left(0,t_f\right]\to\mathbb{R}$ a prescribed, time-dependent, slip velocity along $\partial\Omega$. The prescribed normal velocity is given by $k:\partial\Omega\times\left(0,t_f\right]\to\mathbb{R}$ and satisfies

$$\int_{\partial\Omega} k(\boldsymbol{x},t)\,\mathrm{d}\Gamma = 0\,. \tag{3}$$

The cross product $\times$ in (2) is defined as usual for a 3D domain. Assuming Ω is contained in the xy plane of 3D Euclidean space, given two vectors $\vec{a} = a_x\vec{e}_x + a_y\vec{e}_y$ and $\vec{b} = b_x\vec{e}_x + b_y\vec{e}_y$ in Ω, the cross product results in $\vec{a}\times\vec{b} = (a_xb_y - a_yb_x)\vec{e}_z$. Here, the component in $\vec{e}_z$ is seen as a scalar.

Equation (1) can be written in a variety of different formulations which usually require the nonlinear term to be written in a different manner or introduce the vorticity, defined $\omega = \nabla\times\vec{u}$, as an additional variable [12,13]. All of these alternative formulations are equivalent at the continuous level; however, once the equations are discretized, certain vector calculus identities may no longer hold. Therefore, a fundamental point that must be taken into account is that each of these formulations leads to different discretizations of the Navier–Stokes equations with different properties [30].

The formulation used in the MEEVC scheme [1] is a combination of the momentum equation in the rotational form and the vorticity transport equation in the skew-symmetric form:

$$\begin{cases} \dfrac{\partial\vec{u}}{\partial t} + \omega\times\vec{u} + \nabla\bar{p} = -\nu\nabla\times\omega & \text{in } \Omega\times(0,t_F], \\ \dfrac{\partial\omega}{\partial t} + \dfrac{1}{2}\left(\vec{u}\cdot\nabla\right)\omega + \dfrac{1}{2}\nabla\cdot\left(\vec{u}\omega\right) = \nu\Delta\omega & \text{in } \Omega\times(0,t_F], \\ \nabla\cdot\vec{u} = 0 & \text{in } \Omega\times(0,t_F], \\ \vec{u}\cdot\vec{n} = k(\boldsymbol{x},t), \quad \vec{u}\times\vec{n} = g(\boldsymbol{x},t) & \text{on } \partial\Omega\times(0,t_F], \end{cases} \tag{4}$$

where $\bar{p} := p + \frac{1}{2}\vec{u}\cdot\vec{u}$ is the total pressure and, in 2D, the curl of a vector $\vec{a} = (a_x,a_y)$ is the scalar $\nabla\times\vec{a} = \partial a_y/\partial x - \partial a_x/\partial y$. The curl of the scalar ω, bearing in mind that this is the z-component of the vector $\vec{\omega} = (0,0,\omega)^T$, is $\nabla\times\omega = (\partial\omega/\partial y, -\partial\omega/\partial x)^T$.

Equation (4) was also used by Heister et al. [28] for the construction of a finite element discretization of the 2D incompressible Navier–Stokes equations; a similar formulation for the 3D equations is used by Benzi et al. [26] and by Lee et al. [25]. The main advantage of this formulation is that the rotational and the skew-symmetric forms of the nonlinear terms will not introduce numerical dissipation of kinetic energy and enstrophy, respectively, when used together with exactly divergence-free velocity fields. Furthermore, this formulation allows for the decoupling of the vorticity equation by means of a staggered time integrator.

2.2. Weak formulation

The construction of the finite element discretization of (4) requires these equations to be written in a weak form. Prior to the application of slip boundary conditions, the following weak form is obtained for all $t\in(0,t_F]$:

$$\begin{cases} \text{Find } \vec{u}\in H(\mathrm{div},\Omega),\ p\in L^2(\Omega) \text{ and } \omega\in H(\mathrm{curl},\Omega) \text{ such that:} \\ \langle\dfrac{\partial\vec{u}}{\partial t},\vec{v}\rangle + \langle\omega\times\vec{u},\vec{v}\rangle - \langle\bar{p},\nabla\cdot\vec{v}\rangle + \displaystyle\int_{\partial\Omega}\bar{p}\left(\vec{v}\cdot\vec{n}\right)\,\mathrm{d}\Gamma = -\nu\langle\nabla\times\omega,\vec{v}\rangle, \quad \forall\vec{v}\in H(\mathrm{div},\Omega), \quad \text{(a)} \\ \langle\dfrac{\partial\omega}{\partial t},\xi\rangle - \dfrac{1}{2}\langle\omega,\nabla\cdot(\vec{u}\xi)\rangle + \dfrac{1}{2}\langle\nabla\cdot\left(\vec{u}\omega\right),\xi\rangle + \dfrac{1}{2}\displaystyle\int_{\partial\Omega}\xi\omega(\vec{u}\cdot\vec{n})\,\mathrm{d}\Gamma = \\ -\nu\langle\nabla\times\omega,\nabla\times\xi\rangle + \nu\displaystyle\int_{\partial\Omega}\xi\,(\nabla\times\omega)\times\vec{n}\,\mathrm{d}\Gamma, \quad \forall\xi\in H(\mathrm{curl},\Omega), \quad \text{(b)} \\ \langle\nabla\cdot\vec{u},q\rangle = 0, \quad \forall q\in L^2(\Omega), \quad \text{(c)} \end{cases} \tag{5}$$

where integration by parts has been carried out to obtain the following identities

$$\langle\nabla\bar{p},\vec{v}\rangle = -\langle\bar{p},\nabla\cdot\vec{v}\rangle + \int_{\partial\Omega}\bar{p}\left(\vec{v}\cdot\vec{n}\right)\,\mathrm{d}\Gamma, \tag{6a}$$

$$\langle(\vec{u}\cdot\nabla)\omega,\xi\rangle = -\langle\omega,\nabla\cdot(\vec{u}\xi)\rangle + \int_{\partial\Omega}\xi\omega(\vec{u}\cdot\vec{n})\,\mathrm{d}\Gamma, \tag{6b}$$

$$\langle\Delta\omega,\xi\rangle = -\langle\nabla\times\omega,\nabla\times\xi\rangle + \int_{\partial\Omega}\xi\,(\nabla\times\omega)\times\vec{n}\,\mathrm{d}\Gamma. \tag{6c}$$

In (5) and (6), the angled brackets $\langle\cdot,\cdot\rangle$ represent the $L^2(\Omega)$ inner product of two functions over Ω. The function space $L^2(\Omega)$ contains square integrable functions and the spaces $H(\mathrm{curl},\Omega)$ and $H(\mathrm{div},\Omega)$ contain square-integrable vector functions whose curl and divergence are square-integrable, respectively.

In the theory of Sobolev spaces, the well defined restriction of a general function v to the boundary of the domain is carried out with the trace operator γ [31]. In more practical terms, the strong prescription of boundary conditions on $H(\mathrm{curl},\Omega)$ and $H(\mathrm{div},\Omega)$ is equivalent to equating the trace of its functions to a given value. Therefore, it is useful to know how the trace operator is defined for these spaces. In 3D, the traces of elements of these vector spaces are the tangential and normal vector components at the boundary, respectively. In 2D, the case considered here, $H(\mathrm{curl},\Omega)$ is equivalent to $H^1(\Omega)$, and the trace is defined as the pointwise restriction to $\partial\Omega$, such that $\gamma(\xi)=\xi|_{\partial\Omega}$ for $\xi\in H(\mathrm{curl},\Omega)$.[1]

For $\vec{v}\in H(\mathrm{div},\Omega)$, its trace is defined $\gamma(\vec{v})=\vec{v}\cdot\vec{n}\big|_{\partial\Omega}\in H^{-\frac{1}{2}}(\partial\Omega)$, [11], which is the space of linear functionals acting on the trace of H^1 functions.

2.3. Normal velocity boundary conditions

Searching for the velocity vector $\vec{u}$ in $H(\mathrm{div},\Omega)$ implies weaker smoothness requirements for $\vec{u}$ than assuming $\vec{u}\in\left(H^1(\Omega)\right)^2$. For a finite element space to be contained in $H(\mathrm{div},\Omega)$, it is necessary for the normal vector component through each face to be continuous. In general, the degrees of freedom of $H(\mathrm{div},\Omega)$ conforming elements are calculated in terms of moments of the normal components of the vector along the faces [11,32]. Thus, when considering the prescription of the boundary conditions (2) on $\vec{u}$, only $\vec{u}\cdot\vec{n}$ can be strongly imposed. Therefore, equation (5) takes the following form[2] for all $t\in(0,t_F]$:

$$\begin{cases}
\text{Find } \vec{u}\in H_k(\mathrm{div},\Omega),\ p\in L^2(\Omega) \text{ and } \omega\in H(\mathrm{curl},\Omega) \text{ such that:} & \\
\langle\dfrac{\partial\vec{u}}{\partial t},\vec{v}\rangle + \langle\omega\times\vec{u},\vec{v}\rangle - \langle\bar{p},\nabla\cdot\vec{v}\rangle = -\nu\langle\nabla\times\omega,\vec{v}\rangle, & \forall\vec{v}\in H_0(\mathrm{div},\Omega), \quad \text{(a)} \\
\langle\dfrac{\partial\omega}{\partial t},\xi\rangle - \dfrac{1}{2}\langle\omega,\nabla\cdot(\vec{u}\xi)\rangle + \dfrac{1}{2}\langle\nabla\cdot\left(\vec{u}\omega\right),\xi\rangle + \dfrac{1}{2}\displaystyle\int_{\partial\Omega}\xi\omega k\,\mathrm{d}\Gamma = & \\
-\nu\langle\nabla\times\omega,\nabla\times\xi\rangle + \nu\displaystyle\int_{\partial\Omega}\xi\,(\nabla\times\omega)\times\vec{n}\,\mathrm{d}\Gamma, & \forall\xi\in H(\mathrm{curl},\Omega), \quad \text{(b)} \\
\langle\nabla\cdot\vec{u},q\rangle = 0, & \forall q\in L^2(\Omega), \quad \text{(c)}
\end{cases} \tag{7}$$

with the restricted function space $H_k(\mathrm{div},\Omega)$ defined as

$$H_k(\mathrm{div},\Omega) = \left\{\vec{u}\in H(\mathrm{div},\Omega)\mid\vec{u}\cdot\vec{n}=k(\boldsymbol{x},t) \text{ on } \partial\Omega\right\}, \tag{8}$$

and $H_0(\mathrm{div},\Omega)$ is the space defined in (8) with $k(\boldsymbol{x},t)=0$.

2.4. Vorticity boundary conditions

Once $\vec{u}\cdot\vec{n}$ has been strongly enforced, only the vorticity along the boundary remains to be set such that the resulting tangential velocity along the boundary satisfies the tangential boundary condition $\vec{u}\times\vec{n}=g(\boldsymbol{x},t)$. Equation (7) indicates that two possibilities exist:

1. Given a vorticity ω_Γ defined on $\partial\Omega$, non-homogeneous Dirichlet boundary conditions can be prescribed with $\omega=\omega_\Gamma$ on $\partial\Omega$.
2. Neumann boundary conditions can also be given for the vorticity equation. In this case, the curl of the vorticity along the boundary $\left((\nabla\times\omega)\times\vec{n}\right)_\Gamma$ is known and the boundary integral in (7b) can be determined.

Both the vorticity and its curl along the wall can be calculated with the kinematic condition (9) and with the momentum equation (the dynamic condition), respectively. These two approaches are explored in the following sections.

[1] The same holds for $H(\mathrm{grad},\Omega)$, defined further on.

[2] Note that by imposing $\vec{u}\cdot\vec{n}$ strongly along the boundary means that the test function $\vec{v}\cdot\vec{n}=0$ vanishes along the boundary. This problem is still under-determined because no other boundary conditions have been imposed yet.

2.4.1. Kinematic vorticity boundary conditions

The kinematic condition establishes a linear, instantaneous relation:

$$\tilde{\omega} = \nabla \times \vec{u}. \tag{9}$$

In this case, the vorticity calculated with this equation is renamed $\tilde{\omega}$ in order to distinguish it from the vorticity ω calculated with the vorticity transport equation in (4). Although the equality $\tilde{\omega} = \omega$ holds at the continuous level, both vorticity values will generally differ at the discrete level; hence, distinguishing both is important when constructing the finite element approximation. Taking into account that $\vec{u} \in H(\mathrm{div}, \Omega)$, the curl of $\vec{u}$ is not defined, hence its *weak* curl must be computed. For this reason, $\tilde{\omega}$ will be known as the *approximate* vorticity. In its weak form, (9) can be written in the following manner after integrating by parts:

$$\langle \tilde{\omega}, \tilde{\xi} \rangle = \langle \vec{u}, \nabla \times \tilde{\xi} \rangle - \int_{\partial\Omega} \tilde{\xi}\, g(\boldsymbol{x}, t)\, \mathrm{d}\Gamma, \quad \forall \tilde{\xi} \in H(\mathrm{curl}, \Omega), \tag{10}$$

where $g(\boldsymbol{x}, t) = \vec{u} \times \vec{n}$ is the slip velocity defined along $\partial\Omega$, see (2). Two approaches are suggested for the prescription of kinematic vorticity boundary conditions:

(a) **Kinematic Dirichlet boundary conditions**. The approximate vorticity $\tilde{\omega}$, calculated with (10), can be used to strongly impose the values of ω on each of the nodes of the mesh along $\partial\Omega$. Formally, the resulting boundary value problem with non-homogeneous Dirichlet boundary conditions is written with homogeneous boundary conditions. This can be done by setting the vorticity to $\omega = \omega_0 + \omega'$, with $\omega_0 \in H_0(\mathrm{curl}, \Omega)$, defined as

$$H_0(\mathrm{curl}, \Omega) = \{\omega \in H(\mathrm{curl}, \Omega) \mid \omega = 0 \text{ on } \partial\Omega\}, \tag{11}$$

and ω' is any function in $H(\mathrm{curl}, \Omega)$ such that $\omega' = \tilde{\omega}$ on $\partial\Omega$. The vorticity transport equation is solved for $\omega_0 \in H_0(\mathrm{curl}, \Omega)$, such that

$$\frac{\partial \omega_0}{\partial t} + \frac{1}{2}\left(\vec{u} \cdot \nabla\right)\omega_0 + \frac{1}{2}\nabla \cdot \left(\vec{u}\omega_0\right) = \nu \Delta \omega_0 + f', \tag{12}$$

where

$$f' = -\frac{\partial \omega'}{\partial t} - \frac{1}{2}\left(\vec{u} \cdot \nabla\right)\omega' - \frac{1}{2}\nabla \cdot \left(\vec{u}\omega'\right) + \nu \Delta \omega'. \tag{13}$$

This approach has been used extensively for the prescription of vorticity boundary conditions [22–26].

(b) **Kinematic Neumann boundary conditions**. A second possibility involving the kinematic relation consists in calculating, as before, the vorticity term $\tilde{\omega} = \nabla \times \vec{u}$ in its weak form. This time, $\tilde{\omega}$ is used to compute $\nabla \times \tilde{\omega}$. The values of $\tilde{\omega}$ along the boundary are then used to weakly impose $\nabla \times \omega$ through the boundary term in (7b)

$$\nu \int_{\partial\Omega} \xi \left(\nabla \times \tilde{\omega}\right) \times \vec{n}\, \mathrm{d}\Gamma.$$

Hence, the additional equation (10) is introduced into the system of equations (7) and coupled with the vorticity transport equation (7b) by means of the boundary term.

2.4.2. Dynamic vorticity boundary conditions

Another option is to use the momentum equation to establish a dynamic relation between the curl of ω and the velocity, which involves a nonlinear term and the pressure gradient. The boundary term in (7), usually known as a *vorticity production* term [15,18,19,27], can be written as a function of the velocity and the pressure gradient by means of the momentum equation, such that:

$$\nu(\nabla \times \omega) \times \vec{n} = -\left(\frac{\partial \vec{u}}{\partial t} + \omega \times \vec{u} + \nabla \bar{p}\right) \times \vec{n} \quad \text{on } \partial\Omega. \tag{14}$$

Using (2) and $(\omega \times \vec{u}) \times \vec{n} = \omega(\vec{u} \cdot \vec{n}) = \omega k(\boldsymbol{x}, t)$, (14) can be written as:

$$\nu(\nabla \times \omega) \times \vec{n} = -\omega k - \frac{\partial g}{\partial t} - \nabla \bar{p} \times \vec{n} \quad \text{on } \partial\Omega, \tag{15}$$

Equation (15) associates the vorticity production with the tangential acceleration and pressure gradient along the wall. This equation can be written in a weak form by multiplying by a test function ξ and integrating along $\partial\Omega$:

$$\nu \int_{\partial\Omega} \xi(\nabla \times \omega) \times \vec{n}\, \mathrm{d}\Gamma = -\int_{\partial\Omega} \xi \omega k(\boldsymbol{x}, t)\, \mathrm{d}\Gamma - \int_{\partial\Omega} \xi \frac{\partial g}{\partial t}\, \mathrm{d}\Gamma - \int_{\partial\Omega} \xi\, (\nabla \bar{p} \times \vec{n})\, \mathrm{d}\Gamma, \quad \forall \xi \in H^{-\frac{1}{2}}(\partial\Omega). \tag{16}$$

Here we use the fact that in 2D $(\nabla \times \omega) \times \vec{n} = \nabla\omega \cdot \vec{n} \in H^{\frac{1}{2}}(\partial\Omega)$.

Therefore, the third method, similar to the method proposed by Olshanskii et al. [27] and based upon the dynamic relation given by (16), is suggested for prescribing vorticity boundary conditions.

(c) **Dynamic Neumann boundary conditions**. The computation of the total pressure gradient $\nabla\bar{p}$ along a solid wall presents difficulties because $\bar{p}$ is sought in $L^2(\Omega)$ and interelement continuity is not strongly enforced; this implies that the gradient $\nabla\bar{p}$ is not defined [27].[3] In the current paper, an alternative method is suggested in which a total pressure $\tilde{p}$ is calculated by means of the pressure Poisson equation. If the divergence is applied to the momentum equation, the following expression can be derived,

$$\Delta\tilde{p} = -\nabla \cdot \left(\omega \times \vec{u}\right). \tag{17}$$

In its weak form, (17) can take the following form: find $\tilde{p} \in H(\mathrm{grad}, \Omega)$ such that,

$$\langle \nabla\tilde{p}, \nabla\chi \rangle = \langle \nabla \cdot \left(\omega \times \vec{u}\right), \chi \rangle + \int_{\partial\Omega} \chi \nabla\tilde{p} \cdot \vec{n}\, \mathrm{d}\Gamma, \quad \forall \chi \in H(\mathrm{grad}, \Omega), \tag{18}$$

where $H(\mathrm{grad}, \Omega)$ is the space of scalar functions with a square integrable gradient. The term $\nabla\tilde{p} \cdot \vec{n}$ remains unknown and therefore must be written in terms of the vorticity and the velocity. Taking into account that $\vec{u} \cdot \vec{n}$ is given along $\partial\Omega$, the normal component of the momentum equation restricted to the boundary is:

$$\nabla\tilde{p} \cdot \vec{n} = -\frac{\partial k}{\partial t} - \nu\, (\nabla \times \omega) \cdot \vec{n} - \left(\omega \times \vec{u}\right) \cdot \vec{n} \quad \text{on } \partial\Omega. \tag{19}$$

If this expression for $\tilde{p} \in H(\mathrm{grad}, \Omega)$ is substituted in (18) and integration by parts is performed, the pressure Poisson equation can be written in terms of $\vec{u}$ and ω:

$$\begin{aligned} \langle \nabla\tilde{p}, \nabla\chi \rangle = &-\langle \omega \times \vec{u}, \nabla\chi \rangle - \nu \int_{\partial\Omega} \chi\, (\nabla \times \omega) \cdot \vec{n}\, \mathrm{d}\Gamma \\ &- \int_{\partial\Omega} \chi \frac{\partial k}{\partial t}\, \mathrm{d}\Gamma, \quad \forall \chi \in H(\mathrm{grad}, \Omega). \end{aligned} \tag{20}$$

Therefore, for a given $\vec{u}$ and ω, the pressure $\tilde{p} \in H(\mathrm{grad}, \Omega)$ is calculated and used in (15). It must be noted that enforcing tangential velocity boundary conditions by means of dynamic Neumann boundary conditions requires the computation of an additional Poisson equation. This can signify a potentially significant increase in the computational cost of the scheme.

3. Spatial discretization

Once the weak formulation has been constructed at the continuous level and three different approaches for the inclusion of the tangential velocity boundary conditions through the prescription of vorticity boundary conditions have been suggested, the next step in the finite element discretization of (4) is the spatial discretization. First, a general spatial discretization is performed without specifying the approach that has been taken for the vorticity boundary conditions yet.

3.1. Finite element discretization

The next step is the selection of stable finite element spaces for the discrete velocity $\vec{u}_h$, pressure $\bar{p}_h$ and vorticity ω_h:

$$\vec{u}_h \in U_h \subset H_k(\mathrm{div}, \Omega), \quad \bar{p}_h \in Q_h \subset L^2(\Omega) \quad \text{and} \quad \omega_h \in W_h \subset H\,(\mathrm{curl}, \Omega) \tag{21}$$

In the MEEVC scheme, the velocity finite element space is set to $U_h = \mathrm{RT}_{k,N} = \left\{\vec{v}_h \in \mathrm{RT}_N \mid \vec{v}_h \cdot \vec{n} = k(\boldsymbol{x}, t) \text{ on } \partial\Omega\right\}$, where RT_N denotes the Raviart–Thomas element of degree N [11,32]. The vorticity finite element space is set to the Lagrange elements of degree N, $W_h = \mathrm{CG}_N$, and the pressure space to the discontinuous Lagrange elements of degree $N-1$, $Q_h = \mathrm{DG}_{N-1}$, [32]. Furthermore, the spaces $\mathrm{RT}_{0,N} = \left\{\vec{v}_h \in \mathrm{RT}_N \mid \vec{v}_h \cdot \vec{n} = 0 \text{ on } \partial\Omega\right\}$ and $\mathrm{CG}_{0,N} = \{\xi_h \in \mathrm{CG}_N \mid \xi_h = 0 \text{ on } \partial\Omega\}$ will also be used. These finite elements are defined on rectilinear triangles of arbitrary shape, see Fig. 1.

[3] Just like [27], a solver in which integration by parts is performed on the pressure term in (16) was tested. However, better results were obtained with the method described here.

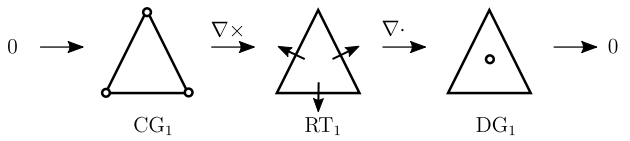

Fig. 1. Scheme of the finite element sequences used for $N = 1$. The degrees of freedom have been marked with circles to indicate point-wise evaluation and with face-wise arrows to indicate integration through an edge. See [33] for a symbolic description of higher order finite element families that form discrete subcomplexes associated to the de Rham complex of differential forms.

This combination of finite element spaces can be proved to form a Hilbert subcomplex in which the differential operators $\nabla\times$ and $\nabla\cdot$ map the elements of each space into the subsequent space, see [1,9,10]. That is,

$$0 \longrightarrow W_h \xrightarrow{\nabla\times} U_h \xrightarrow{\nabla\cdot} Q_h \longrightarrow 0. \tag{22}$$

A discrete subcomplex mimics essential structural properties of the continuous differential equation and therefore its construction is an important requirement for stability and accuracy of a finite element scheme [8]. In this case, two important consequences are the satisfaction of the LBB stability condition [11] and the exact satisfaction of the divergence free constraint for the discrete velocity field $\vec{u}_h$. The De Rham complex implies[4] that we can decompose $\mathrm{RT}_{k,N}$ into a closed subspace $\overset{\circ}{\mathrm{RT}} = \{\vec{v}_h \in \mathrm{RT}_{k,N} \mid \nabla\cdot\vec{v}_h = 0\}$ and its orthogonal complement $\mathcal{N}^T$ such that we have $\mathrm{RT}_{k,N} = \overset{\circ}{\mathrm{RT}} \oplus \mathcal{N}^T$. The map $\nabla\cdot : \mathcal{N}^T \to DG_{N-1}/\mathbb{R}$ is bijective which ensures strong conservation of mass and a pressure field that is determined up to a constant.

Each of the finite element spaces have an associated set of basis functions,

$$U_h = \mathrm{span}\left\{\vec{e}_1^{\,U}, ..., \vec{e}_{d_U}^{\,U}\right\}, \quad Q_h = \mathrm{span}\left\{e_1^{Q}, ..., e_{d_Q}^{Q}\right\} \quad \text{and} \quad W_h = \mathrm{span}\left\{e_1^{W}, ..., e_{d_W}^{W}\right\}, \tag{23}$$

where d_U, d_Q and d_W denote the number of degrees of freedom of each finite element space. The discrete solutions $\vec{u}_h$, $\bar{p}_h$ and ω_h can be expressed as a linear combination of the basis functions

$$\vec{u}_h = \sum_{i=1}^{d_U} u_i \vec{e}_i^{\,U}, \quad \bar{p}_h = \sum_{i=1}^{d_Q} p_i e_i^{Q} \quad \text{and} \quad \omega_h = \sum_{i=1}^{d_W} \omega_i e_i^{W}. \tag{24}$$

The coefficients u_i, p_i and ω_i are the degrees of freedom for velocity, total pressure and vorticity, respectively. In the case of an unsteady flow, these coefficients will be time dependent.

The finite element discretization of (4) consists of solving the following weak formulation:

$$\begin{cases} \text{Find } \vec{u}_h \in \mathrm{RT}_{k,N},\ \bar{p}_h \in \mathrm{DG}_{N-1} \text{ and } \omega_h \in \mathrm{CG}_N \text{ such that:} \\ \langle \dfrac{\partial \vec{u}_h}{\partial t}, \vec{v}_h\rangle + \langle \omega_h \times \vec{u}_h, \vec{v}_h\rangle - \langle \bar{p}_h, \nabla\cdot\vec{v}_h\rangle = -\nu\langle \nabla\times\omega_h, \vec{v}_h\rangle, & \forall \vec{v}_h \in \mathrm{RT}_{0,N}, \quad \text{(a)} \\ \langle \dfrac{\partial \omega_h}{\partial t}, \xi_h\rangle - \dfrac{1}{2}\langle \omega_h, \nabla\cdot\left(\vec{u}_h\xi_h\right)\rangle + \dfrac{1}{2}\langle \nabla\cdot\left(\vec{u}_h\omega_h\right), \xi_h\rangle + \dfrac{1}{2}\displaystyle\int_{\partial\Omega} \xi_h\omega_h k \,\mathrm{d}\Gamma = & \\ -\nu\langle \nabla\times\omega_h, \nabla\times\xi_h\rangle + \nu\displaystyle\int_{\partial\Omega} \xi_h \left(\nabla\times\omega_h\right)\times\vec{n}\,\mathrm{d}\Gamma, & \forall \xi_h \in \mathrm{CG}_N, \quad \text{(b)} \\ \langle \nabla\cdot\vec{u}_h, q_h\rangle = 0, & \forall q_h \in \mathrm{DG}_{N-1}. \quad \text{(c)} \end{cases} \tag{25}$$

The expansions for $\vec{u}_h$, $\bar{p}_h$ and ω_h can be introduced in order to write (25) in a more compact form. If we introduce the vectors $\mathbf{u} := \left[u_1,\ ...,\ u_{d_U}\right]^{\mathrm{T}}$, $\bar{\mathbf{p}} := \left[p_1,\ ...,\ p_{d_Q}\right]^{\mathrm{T}}$ and $\boldsymbol{\omega} := \left[\omega_1,\ ...,\ \omega_{d_W}\right]^{\mathrm{T}}$, (25) can be written in matrix form as

$$\begin{cases} \text{Find } \mathbf{u} \in \mathbb{R}^{d_U},\ \bar{\mathbf{p}} \in \mathbb{R}^{d_Q} \text{ and } \boldsymbol{\omega} \in \mathbb{R}^{d_W} \text{ such that:} \\ \mathbf{M}\dfrac{\mathrm{d}\mathbf{u}}{\mathrm{d}t} + \mathbf{R}\mathbf{u} - \mathbf{P}\bar{\mathbf{p}} = -\nu\boldsymbol{l}, & \text{(a)} \\ \mathbf{N}\dfrac{\mathrm{d}\boldsymbol{\omega}}{\mathrm{d}t} - \dfrac{1}{2}\mathbf{W}\boldsymbol{\omega} + \dfrac{1}{2}\mathbf{W}^{\mathrm{T}}\boldsymbol{\omega} + \dfrac{1}{2}\mathbf{B}\boldsymbol{\omega} = -\nu\mathbf{L}\boldsymbol{\omega} + \nu\boldsymbol{b}, & \text{(b)} \\ \mathbf{D}\mathbf{u} = 0. & \text{(c)} \end{cases} \tag{26}$$

The momentum equation is written in terms of the matrices $\mathbf{M}$, $\mathbf{R}$, $\mathbf{P}$ and of the column vector $\boldsymbol{l}$. The coefficients of these arrays are given by

$$\mathrm{M}_{ij} := \langle \vec{e}_j^{\,U}, \vec{e}_i^{\,U}\rangle,\ \mathrm{R}_{ij} := \langle \omega_h \times \vec{e}_j^{\,U}, \vec{e}_i^{\,U}\rangle,\ \mathrm{P}_{ij} := \langle e_j^{Q}, \nabla\cdot\vec{e}_i^{\,U}\rangle \text{ and } l_i := \langle \nabla\times\omega_h, \vec{e}_i^{\,U}\rangle. \tag{27}$$

[4] Provided (3) holds.

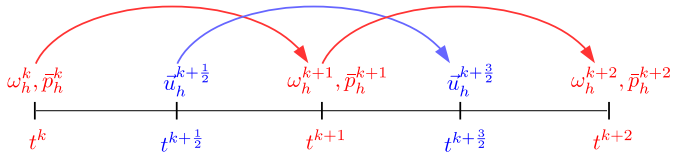

Fig. 2. Diagram of the staggered time step used in the MEEVC scheme.

The vorticity transport equation contains the matrices **N**, **W**, **L**, whose coefficients are given by

$$\mathrm{N}_{ij} := \langle e_j^W, e_i^W \rangle,\ \mathrm{W}_{ij} := \langle e_j^W, \nabla \cdot \left(\vec{u}_h e_i^W \right) \rangle \text{ and } \mathrm{L}_{ij} := \langle \nabla \times e_j^W, \nabla \times e_i^W \rangle, \tag{28}$$

and the matrix **B** and vector $\boldsymbol{b}$, which denote the contribution of the boundary integrals:

$$b_i := \int_{\partial\Omega} e_i^W \, (\nabla \times \omega_h) \times \vec{n} \, \mathrm{d}\Gamma \text{ and } \mathrm{B}_{ij} := \int_{\partial\Omega} e_i^W e_j^W k(\boldsymbol{x}, t) \, \mathrm{d}\Gamma.$$

The divergence-free constraint is written in terms of the matrix **D**, given by the coefficients

$$\mathrm{D}_{ij} := \langle \nabla \cdot \vec{e}_j^U, e_i^Q \rangle = \mathrm{P}_{ji}, \tag{29}$$

such that

$$\mathbf{D} = -\mathbf{P}^T. \tag{30}$$

4. Temporal discretization

The final step in the finite element discretization of (4) is the temporal discretization. Once again, the approach taken for the vorticity boundary conditions is not specified.

The time integrator of polynomial degree one used in the MEEVC scheme is energy conserving and enables the construction of a staggered discretization in time. When applied to the 1D ordinary differential equation

$$\begin{cases} \dfrac{\mathrm{d}f}{\mathrm{d}t} & = g\left(f(t), t\right), \\ f(0) & = f_0, \end{cases} \tag{31}$$

the time integrator of polynomial degree one results in the implicit time stepping scheme

$$\frac{f^k - f^{k-1}}{\Delta t} = g\left(\frac{f^k + f^{k-1}}{2}, t + \frac{\Delta t}{2} \right), \quad k = 1, \ldots, M, \tag{32}$$

where $f^0 = f_0$, Δt is the time step and M the number of steps. This integrator is applied to the semi-discrete system of (26) in the following way: the vorticity ω_h and the total pressure $\bar{p}_h$ are evaluated at t^k, while the velocity $\vec{u}_h$ is computed at the intermediate time instant $t^{k+\frac{1}{2}}$, see Fig. 2. The resulting set of equations takes the following form

$$\begin{cases} \text{Find } \mathbf{u}^{k+\frac{3}{2}} \in \mathbb{R}^{d_U},\ \bar{\mathbf{p}}^{k+1} \in \mathbb{R}^{d_Q} \text{ and } \boldsymbol{\omega}^{k+1} \in \mathbb{R}^{d_W} \text{ such that:} \\ \mathbf{M} \dfrac{\mathbf{u}^{k+\frac{3}{2}} - \mathbf{u}^{k+\frac{1}{2}}}{\Delta t} + \mathbf{R}^{k+1} \dfrac{\mathbf{u}^{k+\frac{3}{2}} + \mathbf{u}^{k+\frac{1}{2}}}{2} - \mathbf{P}\bar{\mathbf{p}}^{k+1} = -\nu \boldsymbol{l}^{k+1}, \\ \mathbf{N} \dfrac{\boldsymbol{\omega}^{k+1} - \boldsymbol{\omega}^k}{\Delta t} + \left(\left(\mathbf{W}^{k+\frac{1}{2}} \right)^{\mathrm{T}} - \mathbf{W}^{k+\frac{1}{2}} + \mathbf{B}^{k+\frac{1}{2}} \right) \dfrac{\boldsymbol{\omega}^{k+1} + \boldsymbol{\omega}^k}{4} = -\nu \mathbf{L} \dfrac{\boldsymbol{\omega}^{k+1} + \boldsymbol{\omega}^k}{2} + \nu \boldsymbol{b}^{k+\frac{1}{2}}, \\ \mathbf{D}\mathbf{u}^{k+\frac{3}{2}} = 0, \end{cases} \tag{33}$$

where the matrix operators are the same as those presented in (27), (28) and (29), with the exception of matrices $\mathbf{R}^{k+1}$ and $\mathbf{W}^{k+\frac{1}{2}}$, defined by the coefficients

$$\mathrm{R}_{ij}^{k+1} := \langle \omega_h^{k+1} \times \vec{e}_j^U, \vec{e}_i^U \rangle \text{ and } \mathrm{W}_{ij}^{k+\frac{1}{2}} := \langle e_j^W, \nabla \cdot \left(\vec{u}_h^{k+\frac{1}{2}} e_i^W \right) \rangle, \tag{34}$$

and vectors $\boldsymbol{l}^{k+1}$ and $\boldsymbol{b}^{k+\frac{1}{2}}$ and matrix $\mathbf{B}^{k+\frac{1}{2}}$ composed of coefficients

$$l_i^{k+1} := \langle \nabla \times \omega_h^{k+1}, \vec{e}_i^{\,U} \rangle,\ b_i^{k+\frac{1}{2}} := \int_{\partial\Omega} e_i^W \left(\nabla \times \omega_h^{k+\frac{1}{2}} \right) \times \vec{n}\, \mathrm{d}\Gamma$$
$$\text{and } \mathrm{B}_{ij}^{k+\frac{1}{2}} := \int_{\partial\Omega} e_i^W e_j^W k(\boldsymbol{x}, t^{k+\frac{1}{2}})\, \mathrm{d}\Gamma. \tag{35}$$

The drawback of computing a nonlinear system of equations is therefore overcome by staggering the variables in time. This implies that instead of solving a non-linear system of $d_U + d_Q + d_W$ variables that requires a series of iterations at each time step, only two linear systems of equations are solved, with d_W and $d_U + d_Q$ variables each. Given the initial conditions, $\vec{u}_h^{\,0}$ and ω_h^0, the initial time step is required to be implicit because $\vec{u}_h^{\,\frac{1}{2}}$ is not known.

5. Numerical schemes

The three approaches for the prescription of vorticity boundary conditions suggested in Section 2.4 lead to 3 different numerical schemes. The resulting schemes, discretized in time and space, are presented in this section. For the kinematic and dynamic solvers, the additional variable $\tilde{\omega}$ and $\tilde{p}$, respectively, is approximated with continuous Lagrange elements of degree N, that is, with CG_N. For brevity we have set $k(\boldsymbol{x}, t) = 0$ in the following sections.

5.1. MEEVC with kinematic Dirichlet boundary conditions

Given $\vec{u}_h^{\,k+\frac{1}{2}}$, $\vec{u}_h^{\,k-\frac{1}{2}}$ and ω_h^k,

Step 1. Find $\tilde{\omega}_h^{k+1} \in \mathrm{CG}_N$ such that:

$$\langle \tilde{\omega}_h^{k+1}, \xi_h \rangle = \langle \left(\frac{3}{2} \vec{u}_h^{\,k+\frac{1}{2}} - \frac{1}{2} \vec{u}_h^{\,k-\frac{1}{2}} \right), \nabla \times \tilde{\xi}_h \rangle - \int_{\partial\Omega} \tilde{\xi}_h g^{k+1}\, \mathrm{d}\Gamma, \quad \forall \tilde{\xi}_h \in \mathrm{CG}_N.$$

Step 2. Find $\omega_h^{k+1} \in \mathrm{CG}_{0,N}$ such that:

$$\langle \frac{\omega_h^{k+1} - \omega_h^k}{\Delta t}, \xi_h \rangle - \frac{1}{2} \langle \frac{\omega_h^{k+1} + \omega_h^k}{2}, \nabla \cdot \left(\vec{u}_h^{\,k+\frac{1}{2}} \xi_h \right) \rangle + \frac{1}{2} \langle \nabla \cdot \left(\vec{u}_h^{\,k+\frac{1}{2}} \frac{\omega_h^{k+1} + \omega_h^k}{2} \right), \xi \rangle =$$
$$-\nu \langle \nabla \times \frac{\omega_h^{k+1} + \omega_h^k}{2}, \nabla \times \xi_h \rangle + \langle f_h'^{\,k+\frac{1}{2}}, \xi_h \rangle, \quad \forall \xi_h \in \mathrm{CG}_{0,N},$$

with $f_h'^{\,k+\frac{1}{2}}$ defined in terms of $\tilde{\omega}_h^{k+1}$ as shown in (13).

Step 3. Find $\left(\vec{u}_h^{\,k+\frac{3}{2}},\ \tilde{p}^{k+1} \right) \in \left(\mathrm{RT}_{0,N},\ \mathrm{DG}_{N-1} \right)$ such that:

$$\begin{cases} \langle \frac{\vec{u}_h^{\,k+\frac{3}{2}} - \vec{u}_h^{\,k+\frac{1}{2}}}{\Delta t}, \vec{v}_h \rangle + \langle \omega_h^{k+1} \times \frac{\vec{u}_h^{\,k+\frac{3}{2}} + \vec{u}_h^{\,k+\frac{1}{2}}}{2}, \vec{v}_h \rangle - \langle \tilde{p}_h^{k+1}, \nabla \cdot \vec{v}_h \rangle = -\nu \langle \nabla \times \omega_h^{k+1}, \vec{v}_h \rangle, & \forall \vec{v}_h \in \mathrm{RT}_{0,N}, \\ \langle \nabla \cdot \vec{u}_h^{\,k+\frac{3}{2}}, q_h \rangle = 0, & \forall q_h \in \mathrm{DG}_{N-1}. \end{cases}$$

5.2. MEEVC with kinematic Neumann boundary conditions

Given $\vec{u}_h^{\,k+\frac{1}{2}}$ and ω_h^k,

Step 1. Find $\tilde{\omega}_h^{k+\frac{1}{2}} \in \mathrm{CG}_N$ such that:

$$\langle \tilde{\omega}_h^{k+\frac{1}{2}}, \tilde{\xi}_h \rangle = \langle \vec{u}_h^{\,k+\frac{1}{2}}, \nabla \times \tilde{\xi}_h \rangle - \int_{\partial\Omega} \tilde{\xi}_h g^{k+\frac{1}{2}}\, \mathrm{d}\Gamma, \quad \forall \tilde{\xi}_h \in \mathrm{CG}_N.$$

Step 2. Find $\omega_h^{k+1} \in \mathrm{CG}_N$ such that:

$$\langle \frac{\omega_h^{k+1} - \omega_h^k}{\Delta t}, \xi_h \rangle - \frac{1}{2} \langle \frac{\omega_h^{k+1} + \omega_h^k}{2}, \nabla \cdot \left(\vec{u}_h^{\,k+\frac{1}{2}} \xi_h \right) \rangle + \frac{1}{2} \langle \nabla \cdot \left(\vec{u}_h^{\,k+\frac{1}{2}} \frac{\omega_h^{k+1} + \omega_h^k}{2} \right), \xi \rangle =$$
$$= -\nu \langle \nabla \times \frac{\omega_h^{k+1} + \omega_h^k}{2}, \nabla \times \xi_h \rangle + \nu \int_{\partial\Omega} \xi_h \left(\nabla \times \tilde{\omega}_h^{k+\frac{1}{2}} \right) \times \vec{n}\, \mathrm{d}\Gamma, \quad \forall \xi_h \in \mathrm{CG}_N.$$

Step 3. Find $\left(\vec{u}_h^{\,k+\frac{3}{2}},\ \bar{p}^{k+1}\right) \in \left(\mathrm{RT}_{0,N},\ \mathrm{DG}_{N-1}\right)$ such that:

$$\begin{cases} \langle \dfrac{\vec{u}_h^{\,k+\frac{3}{2}} - \vec{u}_h^{\,k+\frac{1}{2}}}{\Delta t}, \vec{v}_h \rangle + \langle \omega_h^{k+1} \times \dfrac{\vec{u}_h^{\,k+\frac{3}{2}} + \vec{u}_h^{\,k+\frac{1}{2}}}{2}, \vec{v}_h \rangle - \langle \bar{p}_h^{k+1}, \nabla \cdot \vec{v}_h \rangle = -\nu \langle \nabla \times \omega_h^{k+1}, \vec{v}_h \rangle, & \forall \vec{v}_h \in \mathrm{RT}_{0,N}, \\ \langle \nabla \cdot \vec{u}_h^{\,k+\frac{3}{2}}, q_h \rangle = 0, & \forall q_h \in \mathrm{DG}_{N-1}. \end{cases}$$

5.3. MEEVC with dynamic Neumann boundary conditions

Given $\vec{u}_h^{\,k+\frac{1}{2}}$, ω_h^k and ω_h^{k-1},

Step 1. Find $\tilde{p}_h^{k+\frac{1}{2}} \in \mathrm{CG}_N$ such that:

$$\langle \nabla \tilde{p}_h^{k+\frac{1}{2}}, \nabla \chi_h \rangle = -\langle \bar{\omega}_h^{k+\frac{1}{2}} \times \vec{u}_h^{\,k+\frac{1}{2}}, \nabla \chi_h \rangle - \nu \int_{\partial\Omega} \chi_h \left(\nabla \times \bar{\omega}_h^{k+\frac{1}{2}} \right) \cdot \vec{n} \, \mathrm{d}\Gamma, \quad \forall \chi \in \mathrm{CG}_N,$$

where $\bar{\omega}_h^{k+\frac{1}{2}} = \frac{3}{2}\omega_h^k - \frac{1}{2}\omega_h^{k-1}$.

Step 2. Find $\omega_h^{k+1} \in \mathrm{CG}_N$ such that:

$$\langle \frac{\omega_h^{k+1} - \omega_h^k}{\Delta t}, \xi_h \rangle - \frac{1}{2} \langle \frac{\omega_h^{k+1} + \omega_h^k}{2}, \nabla \cdot \left(\vec{u}_h^{\,k+\frac{1}{2}} \xi_h \right) \rangle + \frac{1}{2} \langle \nabla \cdot \left(\vec{u}_h^{\,k+\frac{1}{2}} \frac{\omega_h^{k+1} + \omega_h^k}{2} \right), \xi \rangle =$$

$$= -\nu \langle \nabla \times \frac{\omega_h^{k+1} + \omega_h^k}{2}, \nabla \times \xi_h \rangle - \int_{\partial\Omega} \xi_h \left[\frac{\partial g}{\partial t} \right]^{k+\frac{1}{2}} \mathrm{d}\Gamma - \int_{\partial\Omega} \xi_h \, (\nabla \tilde{p}_h^{k+\frac{1}{2}} \times \vec{n}) \, \mathrm{d}\Gamma, \quad \forall \xi_h \in \mathrm{CG}_N.$$

Step 3. Find $\left(\vec{u}_h^{\,k+\frac{3}{2}},\ \bar{p}^{k+1}\right) \in \left(\mathrm{RT}_{0,N},\ \mathrm{DG}_{N-1}\right)$ such that:

$$\begin{cases} \langle \dfrac{\vec{u}_h^{\,k+\frac{3}{2}} - \vec{u}_h^{\,k+\frac{1}{2}}}{\Delta t}, \vec{v}_h \rangle + \langle \omega_h^{k+1} \times \dfrac{\vec{u}_h^{\,k+\frac{3}{2}} + \vec{u}_h^{\,k+\frac{1}{2}}}{2}, \vec{v}_h \rangle - \langle \bar{p}_h^{k+1}, \nabla \cdot \vec{v}_h \rangle = -\nu \langle \nabla \times \omega_h^{k+1}, \vec{v}_h \rangle, & \forall \vec{v}_h \in \mathrm{RT}_{0,N}, \\ \langle \nabla \cdot \vec{u}_h^{\,k+\frac{3}{2}}, q_h \rangle = 0, & \forall q_h \in \mathrm{DG}_{N-1}. \end{cases}$$

6. Conservation properties

In the original paper [1] the MEEVC scheme was formulated with periodic boundary conditions. Under these conditions, mass and total vorticity proved to be conserved for all cases. In the case of non-zero viscosity, both kinetic energy and enstrophy will no longer be conserved. The evolution of these quantities will be studied for the three numerical schemes presented in Section 5 with $k(\boldsymbol{x}, t) = 0$ for simplicity.

6.1. Conservation of mass

In (4), conservation of mass is expressed with the divergence-free constraint of the velocity field $\vec{u}_h$. As indicated in Section 3, the use of Raviart–Thomas elements for the velocity exactly enforces this constraint in a point-wise sense. This is valid for all of the schemes.

6.2. Conservation of vorticity

At the continuous level, a flow problem defined with boundary conditions (2) will have a constant total vorticity $\mathcal{W}$ whenever the tangential velocity at the boundary g is independent of time. Integration over Ω of the vorticity yields

$$\int_\Omega \omega \, \mathrm{d}\Omega = -\int_{\partial\Omega} \vec{u} \times \vec{n} \, \mathrm{d}\Gamma = -\int_{\partial\Omega} g \, \mathrm{d}\Gamma = \text{const.}, \tag{36}$$

where the Stokes theorem has been used to relate the integral of the curl of the velocity to the circulation around the boundary of the surface. The same result can be obtained with the vorticity transport equation. Integration over Ω and application of the divergence theorem on the convective and diffusive terms gives

$$\frac{\partial}{\partial t} \int_\Omega \omega \, \mathrm{d}\Omega = \nu \int_{\partial\Omega} \nabla \times \omega \times \vec{n} \, \mathrm{d}\Gamma. \tag{37}$$

The boundary term of (37) can be written in terms of the pressure by restricting the momentum equation to the boundary. This integral will be zero whenever g does not depend on time, that is,

$$\frac{\partial}{\partial t}\int_{\Omega}\omega\,\mathrm{d}\Omega=\nu\int_{\partial\Omega}(\nabla\times\omega)\times\vec{n}\,\mathrm{d}\Gamma=-\int_{\partial\Omega}\nabla\bar{p}\times\vec{n}\,\mathrm{d}\Gamma=0. \tag{38}$$

The final equality in (38) holds whenever Ω is bounded by a closed curve.

Here, conservation of vorticity will be studied for the functions g which satisfy (36) and for domains bounded by closed curves. The discrete conservation of total vorticity can be expressed with the following requirement:

$$\mathcal{W}_h^{k+1}=\int_{\Omega}\omega_h^{k+1}\,\mathrm{d}\Omega:=\langle\omega_h^{k+1},1\rangle=\langle\omega_h^{k},1\rangle:=\int_{\Omega}\omega_h^{k}\,\mathrm{d}\Omega=\mathcal{W}_h^{k}. \tag{39}$$

The time evolution of the total vorticity is governed by the discretized vorticity transport equation, see (33). An explicit expression can be obtained for the special case of $\xi_h=1$:

$$\begin{aligned}&\langle\frac{\omega_h^{k+1}-\omega_h^{k}}{\Delta t},1\rangle-\frac{1}{2}\langle\frac{\omega_h^{k+1}+\omega_h^{k}}{2},\nabla\cdot\vec{u}_h^{\,k+\frac{3}{2}}\rangle+\frac{1}{2}\langle\nabla\cdot\left(\vec{u}_h^{\,k+\frac{3}{2}}\frac{\omega_h^{k+1}+\omega_h^{k}}{2}\right),1\rangle=\\&-\nu\langle\nabla\times\left(\frac{\omega_h^{k+1}+\omega_h^{k}}{2}\right),\nabla\times 1\rangle+\nu\int_{\partial\Omega}\nabla\times\omega_h^{k+\frac{1}{2}}\times\vec{n}\,\mathrm{d}\Gamma.\end{aligned} \tag{40}$$

The exact satisfaction of the divergence-free constraint implies that the second term of (40) is zero. On the other hand, the divergence theorem can be applied to the third term:

$$\langle\nabla\cdot\left(\vec{u}_h^{\,k+\frac{3}{2}}\frac{\omega_h^{k+1}+\omega_h^{k}}{2}\right),1\rangle:=\int_{\Omega}\nabla\cdot\left(\vec{u}_h^{\,k+\frac{3}{2}}\frac{\omega_h^{k+1}+\omega_h^{k}}{2}\right)\mathrm{d}\Omega=\int_{\partial\Omega}\left(\frac{\omega_h^{k+1}+\omega_h^{k}}{2}\right)\vec{u}_h^{\,k+\frac{3}{2}}\cdot\vec{n}\,\mathrm{d}\Gamma. \tag{41}$$

Boundary conditions (2) enforce $\vec{u}\cdot\vec{n}=0$ along $\partial\Omega$ and these are exactly satisfied with $\vec{u}_h\in\mathrm{RT}_{0,N}$. Hence, the third term of (41) is exactly zero. Equation (41) can be rearranged and written as follows:

$$\langle\omega_h^{k+1},1\rangle=\langle\omega_h^{k},1\rangle+\nu\Delta t\int_{\partial\Omega}\nabla\times\omega_h^{k+\frac{1}{2}}\times\vec{n}\,\mathrm{d}\Gamma. \tag{42}$$

Whether vorticity is conserved or not will depend on how the tangential velocity along the boundary is enforced:

1. MEEVC with kinematic Dirichlet boundary conditions. The specification of Dirichlet boundary conditions for the vorticity transport equation requires $\xi_h\in\mathrm{CG}_{0,N}$; this implies that the Equation (42) will not hold for this case because it is only valid for $\xi_h=1\notin\mathrm{CG}_{0,N}$. Numerical test cases in Section 7 confirm that $\mathcal{W}_h$ is not conserved with Dirichlet boundary conditions.
2. MEEVC with kinematic Neumann boundary conditions. The boundary integral in (42) is computed with the *approximate* vorticity, $\tilde{\omega}_h$. This term is computed with the kinematic condition, (10); for $\tilde{\xi}=1$,

$$\langle\tilde{\omega}_h^{k+\frac{1}{2}},1\rangle=\langle\vec{u}_h^{\,k+\frac{1}{2}},\nabla\times 1\rangle-\int_{\partial\Omega}g\,\mathrm{d}\Gamma=\int_{\partial\Omega}g\,\mathrm{d}\Gamma=\text{const.}, \tag{43}$$

   such that the total *approximate* vorticity is conserved. However, this does not ensure the boundary integral in (42) to be zero because (38) is not strongly satisfied.
3. MEEVC with dynamic Neumann boundary conditions. This approach to vorticity boundary conditions has the advantage of strongly satisfying Equation (38). Hence, the boundary integral of $\tilde{p}_h$ around a closed contour will always be zero and (39) will be satisfied.

6.3. Conservation of kinetic energy

Kinetic energy $\mathcal{K}$, together with enstrophy $\mathcal{E}$, is one of the two *secondary* conservation properties of the MEEVC scheme. In the original paper, conservation of $\mathcal{K}$ was proved for $\nu=0$. As will be proved below, the approach taken for the prescription of boundary conditions does not affect conservation of kinetic energy when viscosity is switched off.

At the continuous level, $\mathcal{K}$ is proportional to the $L^2(\Omega)$ norm of the velocity,

$$\mathcal{K}=\frac{1}{2}\left\|\vec{u}\right\|_{L^2(\Omega)}=\frac{1}{2}\langle\vec{u},\vec{u}\rangle. \tag{44}$$

This definition extends to the discrete level:

$$\mathcal{K}_h = \frac{1}{2}\left\|\vec{u}_h\right\|_{L^2(\Omega)} = \frac{1}{2}\langle \vec{u}_h, \vec{u}_h\rangle. \tag{45}$$

Conservation of kinetic energy at the discrete level requires the following equality to hold:

$$\mathcal{K}_h^{k+\frac{1}{2}} = \frac{1}{2}\langle \vec{u}_h^{\,k+\frac{1}{2}}, \vec{u}_h^{\,k+\frac{1}{2}}\rangle = \frac{1}{2}\langle \vec{u}_h^{\,k+\frac{3}{2}}, \vec{u}_h^{\,k+\frac{3}{2}}\rangle = \mathcal{K}_h^{k+\frac{3}{2}}. \tag{46}$$

This equality can be proved to hold by evaluating the momentum equation in its discretised form, see (33), with $\vec{v}_h = \frac{1}{2}\vec{u}^{k+\frac{3}{2}} + \frac{1}{2}\vec{u}^{k+\frac{1}{2}}$:

$$\frac{1}{2}\langle \frac{\vec{u}_h^{\,k+\frac{3}{2}} - \vec{u}_h^{\,k+\frac{1}{2}}}{\Delta t}, \vec{u}_h^{\,k+\frac{3}{2}} + \vec{u}_h^{\,k+\frac{1}{2}}\rangle + \frac{1}{2}\langle \omega_h^{k+1} \times \frac{\vec{u}_h^{\,k+\frac{3}{2}} + \vec{u}_h^{\,k+\frac{1}{2}}}{2}, \vec{u}_h^{\,k+\frac{3}{2}} + \vec{u}_h^{\,k+\frac{1}{2}}\rangle - \frac{1}{2}\langle \vec{p}_h^{k+1}, \nabla\cdot\left(\vec{u}_h^{\,k+\frac{3}{2}} + \vec{u}_h^{\,k+\frac{1}{2}}\right)\rangle = 0. \tag{47}$$

The third term of (47) is identically zero because both $\vec{u}^{k+\frac{3}{2}}$ and $\vec{u}^{k+\frac{1}{2}}$ are divergence free. The second term can be written as follows,

$$\langle \omega_h^{k+1} \times \frac{\vec{u}_h^{\,k+\frac{3}{2}} + \vec{u}_h^{\,k+\frac{1}{2}}}{2}, \vec{u}_h^{\,k+\frac{3}{2}} + \vec{u}_h^{\,k+\frac{1}{2}}\rangle = \langle \omega_h^{k+1} \times \vec{u}_h^{\,k+\frac{3}{2}}, \vec{u}_h^{\,k+\frac{1}{2}}\rangle + \langle \omega_h^{k+1} \times \vec{u}_h^{\,k+\frac{1}{2}}, \vec{u}_h^{\,k+\frac{3}{2}}\rangle \tag{48}$$

Given $\mathcal{B}(\vec{a},\vec{b},\vec{c}) = \langle \vec{a}, \vec{b}\times\vec{c}\rangle$, the identity $\mathcal{B}(\vec{a},\vec{b},\vec{c}) = -\mathcal{B}(\vec{c},\vec{b},\vec{a})$ holds, such that (48) is identically zero. This proves that (46) holds for $\nu = 0$.

6.4. Conservation of enstrophy

The MEEVC scheme was proved to conserve enstrophy $\mathcal{E}$ for the case of periodic boundary conditions and $\nu = 0$, [1]. In this section we demonstrate that, depending on the approach chosen for the prescription of vorticity boundary conditions, enstrophy may or may not be conserved when $\nu = 0$, even though tangential velocity boundary conditions no longer make sense for inviscid flow. As we shall see, if no modifications are made to two of the numerical schemes, certain terms associated to the tangential velocity boundary conditions are included in the discretized equations, violating the conservation of enstrophy.

In the same way as $\mathcal{K}$, enstrophy is defined proportional to the $L^2(\Omega)$ norm of the vorticity,

$$\mathcal{E} = \frac{1}{2}\left\|\omega\right\|_{L^2(\Omega)} = \frac{1}{2}\langle \omega, \omega\rangle, \tag{49}$$

with its discrete counterpart defined as,

$$\mathcal{E}_h = \frac{1}{2}\left\|\omega_h\right\|_{L^2(\Omega)} = \frac{1}{2}\langle \omega_h, \omega_h\rangle. \tag{50}$$

In the same way as (46), conservation of enstrophy at the discrete level requires

$$\mathcal{E}_h^k = \frac{1}{2}\langle \omega_h^k, \omega_h^k\rangle = \frac{1}{2}\langle \omega_h^{k+1}, \omega_h^{k+1}\rangle = \mathcal{E}_h^{k+1}\,, \tag{51}$$

to hold when $\nu = 0$. The identity (51) can be proved to hold whenever the dissipation and the boundary term in (33) are neglected. By substituting $\xi_h = \frac{1}{2}\omega_h^k + \frac{1}{2}\omega_h^{k+1}$ into the discretized vorticity transport equation (see (33)), the following expression is obtained,

$$\begin{aligned}&\frac{1}{2}\langle \frac{\omega_h^{k+1} - \omega_h^k}{\Delta t}, \omega_h^{k+1} + \omega_h^k\rangle - \frac{1}{4}\langle \frac{\omega_h^{k+1} + \omega_h^k}{2}, \nabla\cdot\left(\vec{u}_h^{\,k+\frac{1}{2}}\left(\omega_h^{k+1} + \omega_h^k\right)\right)\rangle \\ &+ \frac{1}{4}\langle \nabla\cdot\left(\vec{u}_h^{\,k+\frac{1}{2}}\frac{\omega_h^{k+1} + \omega_h^k}{2}\right), \omega_h^{k+1} + \omega_h^k\rangle = 0.\end{aligned} \tag{52}$$

The two last terms of (52) are equal with opposing signs; hence, (51) is proved to hold and the discrete enstrophy is conserved for $\nu = 0$. However, this derivation will not be valid for each of the methods to impose the tangential velocity boundary conditions described in Section 5:

1. MEEVC with kinematic Dirichlet boundary conditions. In this case, $\xi_h = \frac{1}{2}\omega_h^k + \frac{1}{2}\omega_h^{k+1} \notin \mathrm{CG}_{0,N}$ and the previous derivation is not valid. Numerical test cases in Section 7 indicate that enstrophy is not conserved when $\nu = 0$.

2. MEEVC with kinematic Neumann boundary conditions. This scheme respects the inviscid flow in such a way that, when $\nu = 0$, both the dissipation term and its associated boundary term tend to zero. Therefore, (52) is valid for the kinematic Neumann boundary conditions.
3. MEEVC with dynamic Neumann boundary conditions. The use of dynamic boundary conditions for the vorticity equation implies that the corresponding boundary term no longer depends explicitly on ν. For the limit $\nu = 0$,

$$\frac{1}{2}\langle\omega_h^{k+1}, \omega_h^{k+1}\rangle = \frac{1}{2}\langle\omega_h^{k}, \omega_h^{k}\rangle - \frac{\Delta t}{2}\int_{\partial\Omega}\left(\omega_h^{k} + \omega_h^{k+1}\right)\left(\left[\frac{\partial g}{\partial t}\right]^{k+\frac{1}{2}} + \nabla\tilde{p}_h^{k+\frac{1}{2}} \times \vec{n}\right)\mathrm{d}\Gamma. \tag{53}$$

Equation (53) indicates that not only is enstrophy not exactly conserved, but also that g still enters the equation even though $\nu = 0$.

7. Numerical test cases

In this section, two numerical test cases are computed with the three schemes that have been introduced in Section 5. The first test is the Taylor–Green vortex, for which an analytical solution is known and convergence rates for the discrete velocity, vorticity and pressure errors can be obtained. The second test is the dipole collision at $\mathrm{Re} = 625$.

7.1. Taylor–Green vortex. Order of accuracy of the schemes

The Taylor–Green vortex is a suitable analytical solution for testing the order of accuracy of a scheme. The solution is given by:

$$\begin{cases} u_x(x, y, t) = -\sin(\pi x)\cos(\pi y)e^{-2\pi^2\nu t}, \\ u_y(x, y, t) = \cos(\pi x)\sin(\pi y)e^{-2\pi^2\nu t}, \\ p(x, y, t) = \dfrac{1}{4}\left(\cos(2\pi x) + \cos(2\pi y)\right)e^{-4\pi^2\nu t}, \\ \omega(x, y, t) = -2\pi\sin(\pi x)\sin(\pi y)e^{-2\pi^2\nu t}. \end{cases} \tag{54}$$

This test case was also used in the previous paper [1] with periodic boundary conditions. For the current study, the solution is defined on a domain $\Omega = [0, 2] \times [0, 2]$ and the boundary conditions are assumed to correspond with $\vec{u} = (u_x, u_y)$ on $\partial\Omega$; therefore, $\vec{u} \cdot \vec{n} = 0$ and $g = g(x, y, t) = (u_x, u_y) \times \vec{n}$. The kinematic viscosity is set to $\nu = 0.01$ and the solution is evolved from $t = 0$ to $t = 1$.

The variation of the $H(\mathrm{div}, \Omega)$ errors[5] for $\vec{u}$, the $L^2(\partial\Omega)$ errors for the tangential component of $\vec{u}$, the $L^2(\Omega)$ and $H(\mathrm{curl}, \Omega)$ errors for ω and the $L^2(\Omega)$ errors for p are considered for the three schemes suggested in Section 5. Calculations are carried out for the polynomial degrees $N = 1,\ 2$ and 4, for which the time steps $\Delta t = 5 \times 10^{-3},\ 1 \times 10^{-3}$ and 1×10^{-4} are used, respectively, such that the error introduced by the time integration is very small. The errors are calculated at $t = 1$ and are plotted in Fig. 3. The orders of convergence, which can be found in Tables 1, 2 and 3, have been calculated for each solver and all polynomial orders. These also include the orders of convergence obtained with the MEEVC scheme with periodic boundary conditions for the $L^2(\Omega)$ errors of the velocity and the vorticity. For $\vec{u}_h$, order N was obtained, while convergence rates of $N + 1$ were obtained for ω_h. Therefore the convergence rates for velocity and vorticity are optimal.

The results indicate that the solution with the dynamic Neumann boundary conditions does not converge to the exact solution. Both of the kinematic boundary conditions yield convergence rates for the velocity equivalent to those obtained with periodic boundary conditions. Convergence rates of order N are also obtained for the tangential component of the velocity, indicating that the kinematic Dirichlet and Neumann schemes solve the problem posed in this paper: imposing tangential velocity boundary conditions. Converges rates of order N are also obtained for the $L^2(\Omega)$ pressure errors for the two kinematic solvers.

Regarding the vorticity, the reference convergence rate for the $L^2(\Omega)$ norm is almost obtained for the kinematic Neumann boundary conditions when $N = 2$; for $N = 1$ and 4, this method yields rates of order N. A reduction in rates of 1 order is obtained for the $H(\mathrm{curl}, \Omega)$ norm. These convergence rates are the highest of the three methods proposed in this paper. For the kinematic Dirichlet boundary conditions, the convergence rates are of order $N - 0.5$ for $N = 2$ and 4. This could be related to previous results from Lee et al. [25] and Benzi et al. [26], which report that kinematic Dirichlet boundary conditions introduce numerical errors into the boundary vorticity, propagating further into the domain throughout the computation, resulting in order reduction.

Finally, in order to study the amount of viscous dissipation introduced by the schemes, the decay rates of the kinetic energy $\mathcal{K}(t)$ with time are presented in Fig. 4 and Table 4 and compared with the exact solution. Taking into account the expression of $\vec{u}$ in (54), we have

[5] Since the solution will be point-wise divergence free we have $\|\vec{u}\|_{H(\mathrm{div},)} = \|\vec{u}\|_{L^2}$.

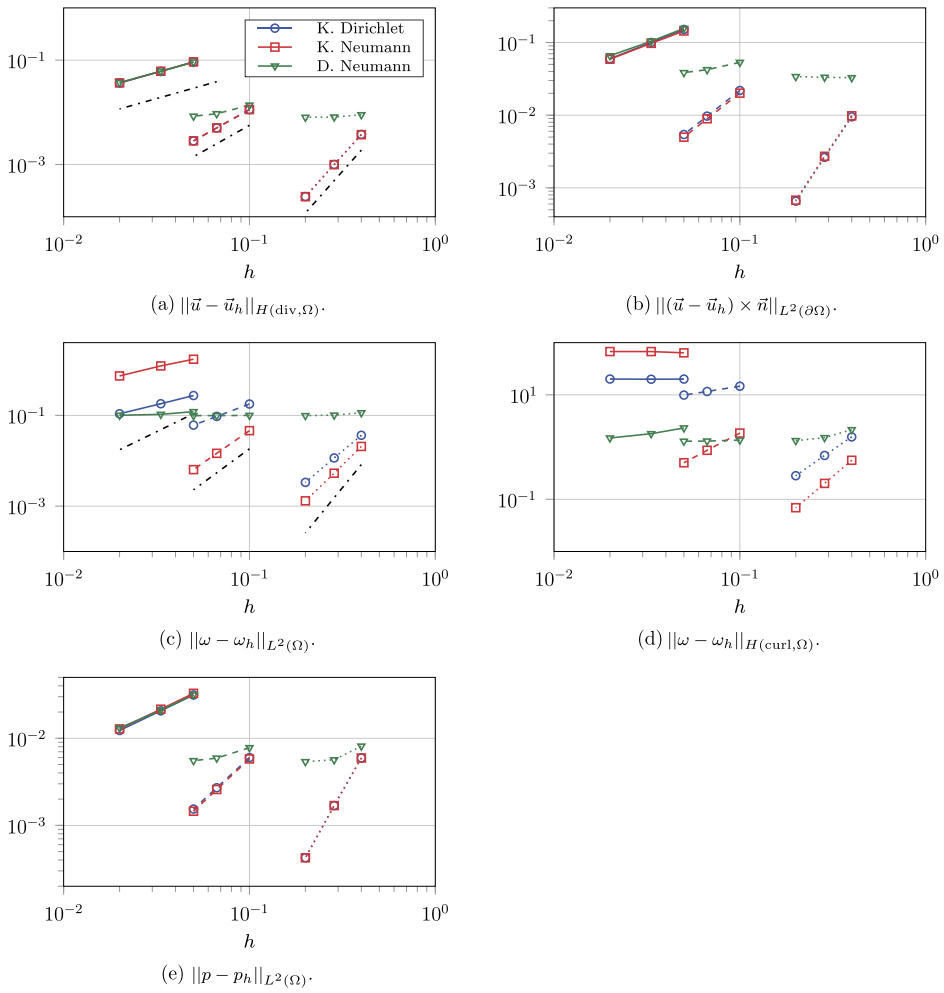

Fig. 3. h-convergence of velocity, vorticity and pressure errors for different polynomial degrees N. Calculations have been carried out for the three schemes suggested in Section 5. Legend: N = 1, N = 2, N = 4, rates obtained with the MEEVC scheme with periodic boundary conditions.

Table 1
Orders of convergence of the velocity error in the $H(\mathrm{div},\Omega)$ norm and for its tangential component in the $L^2(\partial\Omega)$ norm. Results obtained with periodic boundary conditions are also included as a reference.

	$\|\|\vec{u}-\vec{u}_h\|\|_{H(\mathrm{div},\Omega)}$			$\|\|(\vec{u}-\vec{u}_h)\times\vec{n}\|\|_{L^2(\partial\Omega)}$		
	$N=1$	$N=2$	$N=4$	$N=1$	$N=2$	$N=4$
Kinematic Dirichlet	1.00	1.99	3.95	1.01	2.01	3.85
Kinematic Neumann	1.01	1.98	3.94	0.97	2.01	3.85
Dynamic Neumann	0.99	0.70	0.16	0.95	0.47	0.05
Periodic b.c.	1.05	1.97	3.92	–	–	–

$$\mathcal{K}(t) = K\exp(-4\pi^2 t\nu)$$

where $K=1$ is a constant that results from integrating an expression that only depends on (x, y) over the domain. Hence, the decay rate from $t=0$ to $t=1$ is given by

$$\ln(\mathcal{K}(1)) - \ln(\mathcal{K}(0)) = -4\pi^2\nu = -0.3947.$$

Fig. 4 and Table 4 indicate that the two kinematic solvers are highly accurate in calculating the decay of kinetic energy.

Table 2
Orders of convergence of the vorticity error in the $L^2(\Omega)$ and $H(\text{curl}, \Omega)$ norms. Results obtained with periodic boundary conditions are also included as a reference.

	$\|\|\omega - \omega_h\|\|_{L^2(\Omega)}$			$\|\|\omega - \omega_h\|\|_{H(\text{curl},\Omega)}$		
	$N=1$	$N=2$	$N=4$	$N=1$	$N=2$	$N=4$
Kinematic Dirichlet	1.02	1.54	3.44	0.00	0.50	2.48
Kinematic Neumann	0.92	2.85	3.98	0.12	1.89	3.01
Dynamic Neumann	0.20	0.02	0.20	0.53	0.15	0.75
Periodic b.c.	1.87	3.19	5.02	–	–	–

Table 3
Orders of convergence of the pressure error in the $L^2(\Omega)$ norm.

	$\|\|p - p_h\|\|_{L^2(\Omega)}$		
	$N=1$	$N=2$	$N=4$
Kinematic Dirichlet	1.02	1.96	3.81
Kinematic Neumann	1.02	1.99	3.81
Dynamic Neumann	0.95	0.49	0.59

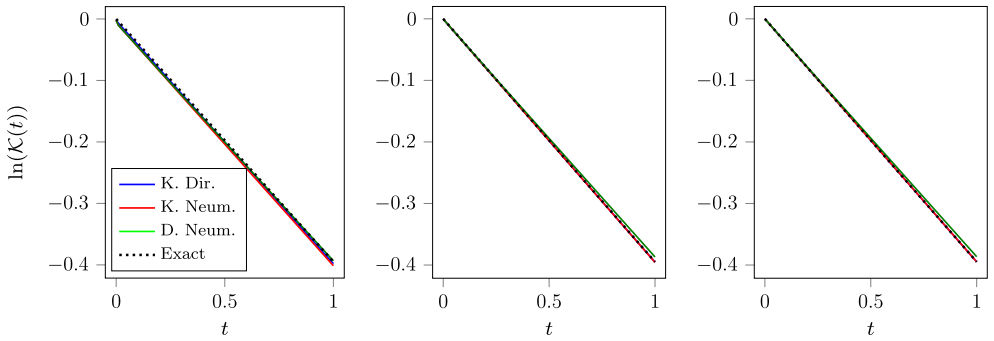

(a) $N = 1$, $h = 0.02$. (b) $N = 2$, $h = 0.05$. (c) $N = 4$, $h = 0.2$.

Fig. 4. Variation of the (natural logarithm of the) kinetic energy $\mathcal{K}(t) = \int_\Omega u^2(t)$.

Table 4
Decay rates for the natural logarithm of the kinetic energy with time.

	$N=1$, $h=0.02$	$N=2$, $h=0.05$	$N=4$, $h=0.2$
Kinematic Dirichlet	−0.3956	−0.3952	−0.3948
Kinematic Neumann	−0.3991	−0.3955	−0.3948
Dynamic Neumann	−0.3911	−0.3868	−0.3865
Exact		−0.3947	

7.2. Dipole collision

Here, results are shown for the normal dipole collision, a test case consisting of a self-propelled vorticity dipole which collides against a wall. This test case was originally proposed for the quantification of vorticity produced in boundary layers [34]. Therefore, this flow problem is an ideal test case for evaluating the different methods for prescribing vorticity boundary conditions suggested in this work.

The results computed in this section are for $\text{Re} = 625$, in a domain $\Omega = [1, 1] \times [-1, 1]$ and for times $t = 0$ to $t = 1$, see Fig. 5. No-slip boundary conditions, $\vec{u} = 0$, are prescribed along the boundary. The initial vorticity distribution for each monopole is given by

$$\omega_0 = \omega_e \left(1 - \left(\frac{r}{r_0}\right)^2\right) \exp\left(-\left(\frac{r}{r_0}\right)^2\right), \tag{55}$$

where r is the distance from the center of the monopole, r_0 its dimensionless radius and ω_e its dimensionless extremum vorticity. Following Clercx and Bruneau [34], the value $r_0 = 0.1$ is taken for both monopoles and $\{\omega_{e,1},\ \omega_{e,2}\} = \{320,\ -320\}$. The initial position of both monopoles is $\{(x_1, y_1),\ (x_2, y_2)\} = \{(0, 0.1),\ (0, -0.1)\}$.

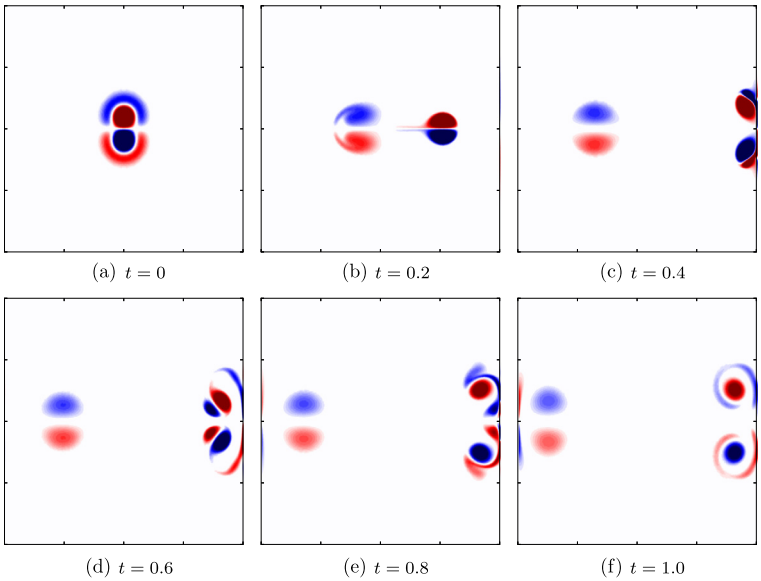

Fig. 5. The normal dipole collision for $\mathrm{Re} = 625$ in a domain $\Omega = [1, 1] \times [-1, 1]$, from $t = 0$ to $t = 1$, obtained with the MEEVC scheme with kinematic Neumann boundary conditions for $N = 2$ and 5210 elements.

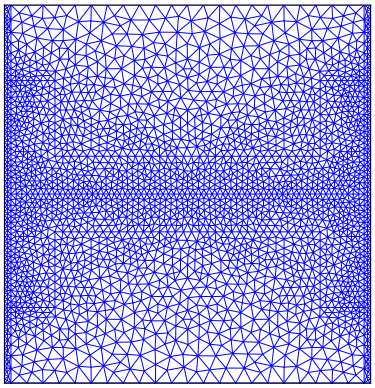

Fig. 6. Unstructured mesh used for the computation of the dipole collision for $\mathrm{Re} = 625$.

Comparisons are made with the benchmark results given by Clercx and Bruneau [34]. The benchmark results are computed with a finite difference scheme in $(\vec{u}, p)$ formulation with N_{FD} equidistant cells along each direction and with a pseudospectral Chebyshev method in $(\vec{u}, \omega, p)$ formulation with N_{SM} collocation points in each direction.

7.2.1. Comparison of the numerical schemes

The performance of each of the solvers proposed in Section 5 is evaluated by computing the normal dipole collision test case. The results presented have been computed with 5210 cells of polynomial degree $N = 2$, see Fig. 6, such that 10645, 26274 and 15630 degrees of freedom are assigned to the discrete vorticity, velocity and pressure variables, respectively. Regarding the time discretization, a time step of $\Delta t = 5 \times 10^{-4}$ is used.

In Fig. 7, the vorticity contour of the region $0.4 \leq x \leq 1$ and $0 \leq y \leq 0.6$ is plotted (the upper-right part of the domain, see Fig. 5f for the vorticity distribution in Ω at $t = 1$); these contours are compared to the contour computed by Clercx and Bruneau with a high order spectral method ($N_{SM} = 256$). From Fig. 7 we see that the dynamic Neumann boundary conditions introduce visible errors in the region close to the boundary. The two other solvers, however, present very similar results to those of the reference.

Fig. 8 shows the variation of the discrete kinetic energy $\mathcal{K}_h$, enstrophy $\mathcal{E}_h$ and palinstrophy $\mathcal{P}_h$. These integral variables are compared to the results from Clercx and Bruneau at $t = 0.25,\ 0.5$ and 0.75. The exact numerical values of these quantities at this time instants are given in Table 5.

The palinstrophy is given by

$$\mathcal{P}_h = \frac{1}{2}\langle \nabla \times \omega_h, \nabla \times \omega_h \rangle, \tag{56}$$

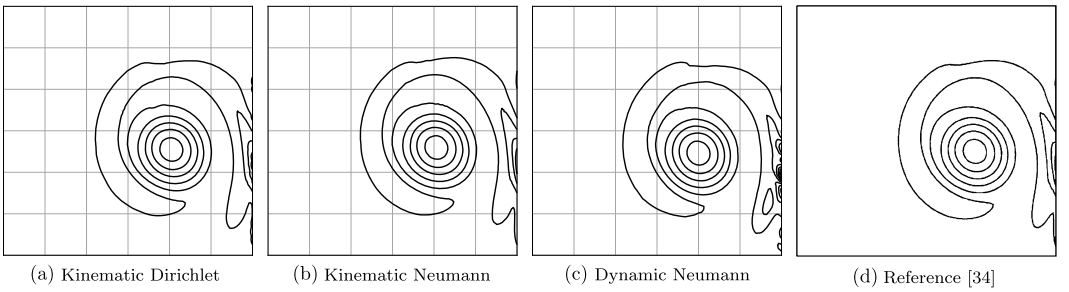

(a) Kinematic Dirichlet (b) Kinematic Neumann (c) Dynamic Neumann (d) Reference [34]

Fig. 7. Vorticity contour plots for the dipole collision at $t = 1$, for the region $0.4 \leq x \leq 1$ and $0 \leq y \leq 0.6$. The contours have been plotted for the vorticity levels $(150, 130, ..., 30, 10, -10, -30, ..., -130, -150)$.

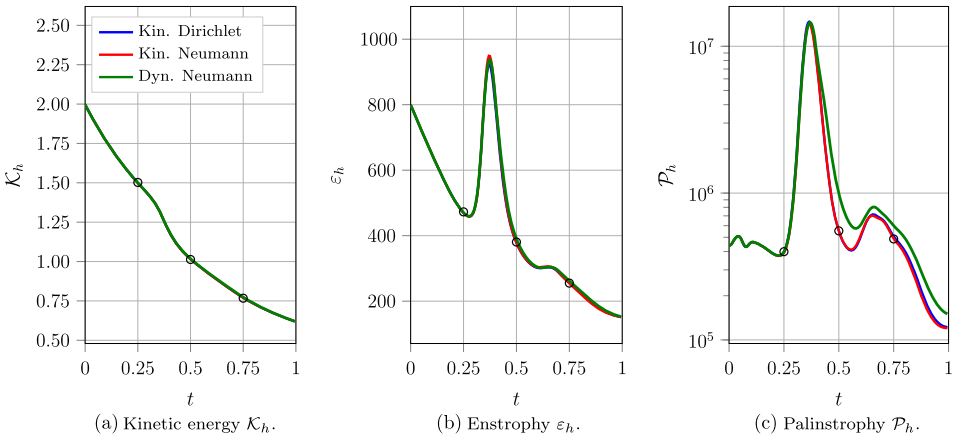

(a) Kinetic energy $\mathcal{K}_h$. (b) Enstrophy ε_h. (c) Palinstrophy $\mathcal{P}_h$.

Fig. 8. Variation over time of the kinetic energy, enstrophy and palinstrophy. Comparisons are made with the results given in [34] at $t = 0.25,\ 0.5$ and 0.75 $(\circ)$.

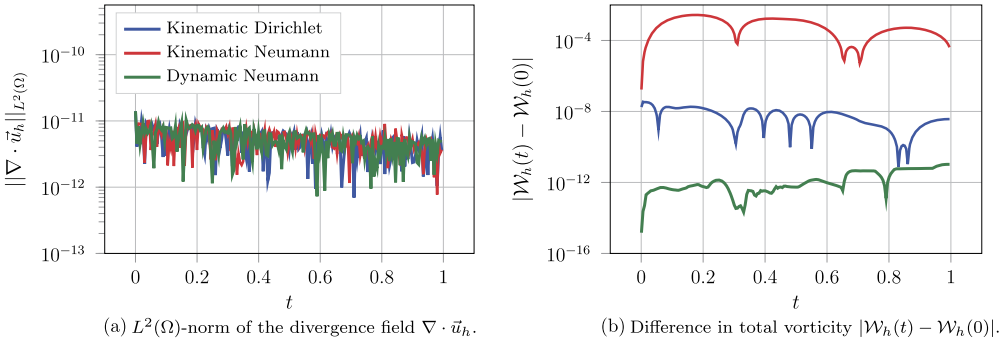

(a) $L^2(\Omega)$-norm of the divergence field $\nabla \cdot \vec{u}_h$. (b) Difference in total vorticity $|\mathcal{W}_h(t) - \mathcal{W}_h(0)|$.

Fig. 9. Variation over time of the $L^2(\Omega)$-norm of the divergence field, $||\nabla \cdot \vec{u}_h||_{L^2(\Omega)}$, and the difference in vorticity $|\mathcal{W}_h(t) - \mathcal{W}_h(0)|$.

such that $\mathcal{P}_h$ depends on the curl of the vorticity in Ω and is much more sensitive to approximation errors than the enstrophy. Fig. 8c clearly shows that the palinstrophy obtained with dynamic Neumann boundary conditions differs from the results given by the reference and the two remaining methods after the first maximum. The first maximum coincides approximately with the moment of the first collision, when large variations in the wall vorticity occur.

The variation with time of the total vorticity $\mathcal{W}_h$ and the $L^2(\Omega)$-norm of the divergence field, $||\nabla \cdot \vec{u}_h||_{L^2(\Omega)}$, are plotted in Fig. 9. The divergence field is solved up to the tolerance set for the iterative solver of the linear system and is very close to machine precision. Regarding the vorticity, taking into account that $\vec{u} = 0$ on $\partial\Omega$, the total vorticity $\mathcal{W}$ should be conserved for all t. As expected, the MEEVC scheme with dynamic Neumann boundary conditions satisfies this requirement at the discrete level, while the two kinematic methods do not. This result confirms that kinematic Dirichlet boundary conditions do not conserve $\mathcal{W}_h$.

More valuable insight into the performance of the different schemes can be obtained when observing the vorticity at the wall. In Fig. 10, the vorticity values at $x = 1$ and $-0.6 \leq y \leq 0$ (lower region of the right wall) are plotted for three different time instants and compared with the results from the reference. The results obtained for the kinematic Neumann

Table 5
Values of the kinetic energy $\mathcal{K}_h$, enstrophy $\mathcal{E}_h$ and palinstrophy $\mathcal{P}_h$ at $t = 0.25$ 0.5 and 0.75. (*) DoF represents the number of degrees of freedom (for ω_h in the case of the MEEVC) along each direction for the finest grid used.

Method	DoF (*)	t	$\mathcal{K}_h$	$\mathcal{E}_h$	$\mathcal{P}_h$
Kinematic Dirichlet	132	0.25	1.5002	469.7	3.97×10^5
		0.5	1.0155	378.1	5.53×10^5
		0.75	0.7708	255.2	5.08×10^5
Kinematic Neumann	132	0.25	1.5002	469.3	3.91×10^5
		0.5	1.0153	378.7	5.55×10^5
		0.75	0.7701	254.1	4.91×10^5
Dynamic Neumann	132	0.25	1.5002	470.2	3.97×10^5
		0.5	1.0184	390.9	9.98×10^5
		0.75	0.7737	261.8	6.00×10^5
$N_{SM} = 256$ (reference)	256	0.25	1.5022	472.6	3.99×10^5
		0.5	1.0130	380.6	5.53×10^5
		0.75	0.7673	255.2	4.87×10^5
$N_{FD} = 1024$ (reference)	1024	0.25	1.502	472.7	3.91×10^5
		0.5	1.013	380.4	5.49×10^5
		0.75	0.767	255.0	4.73×10^5

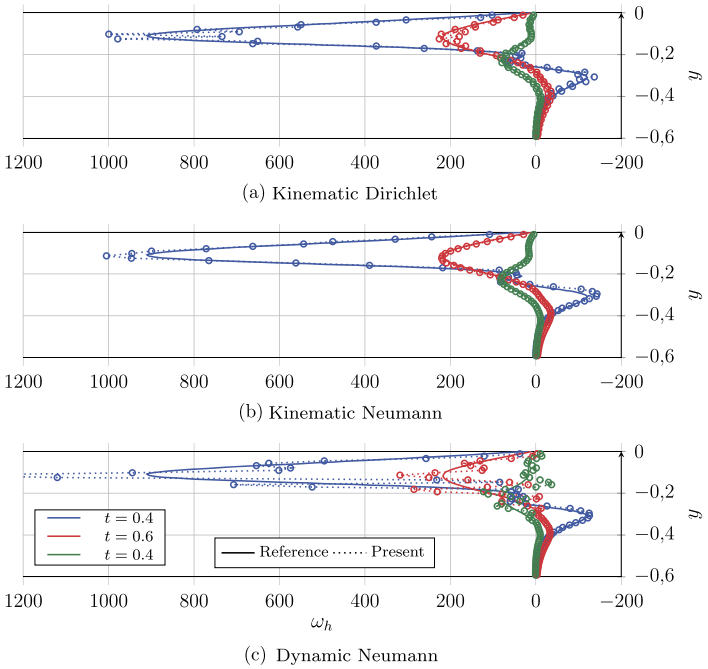

(a) Kinematic Dirichlet

(b) Kinematic Neumann

(c) Dynamic Neumann

Fig. 10. Vorticity distribution at $x = 1$ and $-0.6 \leq y \leq 0$ (lower region of the right wall). The wall vorticity has been plotted for each solver at $t = 0.4$, 0.6 and 1 and is compared to the results given in [34].

boundary conditions show smooth curves which differ from the reference curve in a considerable amount for $t = 0.4$ (more or less the instant of the first collision). This result contrasts with those obtained with the kinematic Dirichlet and dynamic Neumann boundary conditions; in these cases, the vorticity can be seen to oscillate around the reference curve, indicating a possible existence of spurious vorticity modes at the boundary. The oscillations are much greater for the case of the dynamic boundary conditions and seem to explain the existence of ripples which can be appreciated towards the wall in Fig. 7c.

8. Conclusions

This work presents three possibilities for the prescription of slip boundary conditions for the MEEVC scheme, a 2D incompressible flow solver introduced by Palha and Gerritsma [1]. The use of Raviart-Thomas elements for the velocity implies that the tangential component of the velocity along the boundary must be prescribed by means of vorticity boundary

conditions. The three methods are therefore based on local relations between vorticity and velocity (integral approaches are ignored in this work). Of those methods, two are based on the kinematic relation, $\omega = \nabla \times \vec{u}$, and the remaining one on the tangential component of the momentum equation (a dynamic relation). Furthermore, one of the kinematic approaches and the dynamic approach make use of Neumann boundary conditions (weak imposition), while the other kinematic approach specifies the vorticity values in a Dirichlet manner.

The use of the momentum equation in the prescription of vorticity boundary conditions is a choice of interest because it is capable of exactly representing the necessary conditions for exact vorticity conservation. This requires that the pressure or total pressure belong to $H^1(\Omega)$, a condition which is not fulfilled in the MEEVC scheme. As an alternative, the calculation of a new total pressure $\tilde{p} \in H^1(\Omega)$ by means of the pressure Poisson equation is suggested. However, the numerical results obtained in Section 7 indicate that this method does not converge to the correct solution.

The MEEVC scheme with both the kinematic Dirichlet and Neumann boundary conditions yields optimal convergence rates for the velocity and pressure when testing the Taylor–Green vortex. Furthermore, almost no differences can be found between the two resulting velocity fields. However, a slight deterioration in the convergence rate of the vorticity is found for the kinematic Dirichlet boundary conditions. The results obtained from the dipole collision indicate that, unlike the case with kinematic Neumann boundary conditions, oscillations around the reference result are found when using the Dirichlet boundary conditions.

These results suggest that the kinematic Neumann boundary conditions are the most appropriate approach for prescribing boundary conditions for the MEEVC scheme. A clear disadvantage of this approach is the fact that the total vorticity cannot be conserved.

References

[1] A. Palha, M.I. Gerritsma, A mass, energy, enstrophy and vorticity conserving (MEEVC) mimetic spectral element discretization for the 2D incompressible Navier–Stokes equations, J. Comput. Phys. 328 (2017) 200–220.
[2] C.J. Budd, M.D. Piggott, Geometric integration and its applications, Handb. Numer. Anal. 11 (2003) 35–139.
[3] S.H. Christiansen, H.Z. Munthe-Kaas, B. Owren, Topics in structure-preserving discretization, Acta Numer. 20 (2011) 1–119.
[4] J.B. Perot, Discrete conservation properties of unstructured mesh schemes, Annu. Rev. Fluid Mech. 43 (2011) 229–318.
[5] R.W.C.P. Verstappen, A.E.P. Veldman, Symmetry-preserving discretization of turbulent flow, J. Comput. Phys. 187 (2003) 343–368.
[6] L.G. Rebholz, Conservation laws of turbulence models, J. Math. Anal. Appl. 326 (2007) 33–45.
[7] P. Bochev, M. Hyman, Principles of Mimetic Discretizations, IMA, vol. 142, Springer Verlag, 2006, pp. 89–119.
[8] A. Palha, P.P. Rebelo, R. Hiemstra, J. Kreeft, M.I. Gerritsma, Physics-compatible discretization techniques on single and dual grids, with application to the Poisson equation of volume forms, J. Comput. Phys. 257 (2014) 1394–1422.
[9] D.N. Arnold, R.S. Falk, R. Winther, Finite element exterior calculus, homological techniques and applications, Acta Numer. 15 (2006) 1–155.
[10] D.N. Arnold, R.S. Falk, R. Winther, Finite element exterior calculus: from Hodge theory to numerical stability, Bull. Am. Math. Soc. 42 (2010) 281–354.
[11] F. Brezzi, M. Fortin, Mixed and Hybrid Finite Element Methods, vol. 15, Springer Series in Computational Mathematics, vol. 44, Springer, 1991.
[12] P.M. Gresho, Incompressible fluid dynamics: some fundamental formulation issues, Annu. Rev. Fluid Mech. 23 (1991) 413–453.
[13] T.B. Gatski, Review of incompressible fluid flow computations using the vorticity–velocity formulation, Appl. Numer. Math. 7 (1991) 227–239.
[14] J.Z. Wu, J.M. Wu, Vorticity dynamics on boundaries, Adv. Appl. Mech. 32 (1996) 119–275.
[15] M.J. Lighthill, Introduction: boundary layer theory. Chapter II, in: L. Rosenhead (Ed.), Laminar Boundary Layers, Oxford at the Clarendon Press, 1963.
[16] A.J. Chorin, Vortex sheet approximation of boundary layers, J. Comput. Phys. 27 (1978) 428–442.
[17] J.C. Wu, Fundamental solutions and numerical methods for flow problems, Int. J. Numer. Methods Fluids 4 (1984) 185–201.
[18] B.R. Morton, The generation and decay of vorticity, Geophys. Astrophys. Fluid Dyn. 28 (1984) 277–308.
[19] J.Z. Wu, H.Y. Ma, M.D. Zhou, Vorticity and Vortex Dynamics, Springer, Berlin, 2006.
[20] J.Z. Wu, X.H. Wu, H.Y. Ma, J.M. Wu, Dynamic vorticity condition: theoretical analysis and numerical implementation, Int. J. Numer. Methods Fluids 19 (1994) 905–938.
[21] C. Taylor, P. Hood, A numerical solution of the Navier–Stokes equations using the finite element technique, Comput. Fluids 1 (1973) 73–100.
[22] G. Guevremont, W. Habashi, M. Hafez, Finite element solution of the Navier–Stokes equations by a velocity–vorticity method, Int. J. Numer. Methods Fluids 11 (1990) 611–675.
[23] G. Guevremont, W. Habashi, P. Kotiuga, M. Hafez, Finite element solution of the 3D compressible Navier–Stokes equations by a velocity–vorticity method, J. Comput. Phys. 107 (1993) 176–187.
[24] M.A. Olshanskii, L.G. Rebholz, Velocity–vorticity–helicity formulation and a solver for the Navier–Stokes equations, J. Comput. Phys. 229 (2010) 4291–4303.
[25] H.K. Lee, M.A. Olshanskii, L.G. Rebholz, On error analysis for the 3D Navier–Stokes equations in velocity–vorticity–helicity form, SIAM J. Numer. Anal. 49 (2011) 711–732.
[26] M. Benzi, M.A. Olshanskii, L.G. Rebholz, Z. Wang, Assessment of a vorticity based solver for the Navier–Stokes equations, Comput. Methods Appl. Mech. Eng. 247–248 (2012) 216–225.
[27] M.A. Olshanskii, T. Heister, L.G. Rebholz, K.J. Galvin, Natural vorticity boundary conditions on solid walls, Comput. Methods Appl. Mech. Eng. 297 (2015) 18–37.
[28] T. Heister, M.A. Olshanskii, L.G. Rebholz, Unconditional long-time stability of a velocity–vorticity method for the 2D Navier–Stokes equations, Numer. Math. 135 (2017) 143–167.
[29] J. Trujillo, G. Karniadakis, A penalty method for the velocity–vorticity formulation, J. Comput. Phys. 149 (1999) 32–58.
[30] S. Charnyi, T. Heister, M.A. Olshanskii, L.G. Rebholz, On conservation laws of Navier–Stokes Galerkin discretizations, J. Comput. Phys. 337 (2017) 289–308.
[31] S. Brenner, R. Scott, The Mathematical Theory of Finite Element Methods, 2007.
[32] C. Kirby, A. Logg, M.E. Rognes, A.R. Terrel, Common and unusual finite elements, in: Automated Solution of Differential Equations by the Finite Element Method, in: Lecture Notes in Computational Science and Engineering, vol. 84, Springer, 2012, pp. 95–119.
[33] D.N. Arnold, Spaces of finite element differential forms, in: U. Gianazza, F. Brezzi, P.C. Franzone, G. Gilardi (Eds.), Analysis and Numerics of Partial Differential Equations, Springer, 2013, pp. 117–140.
[34] H.J.H. Clercx, C.H. Bruneau, The normal and oblique collision of a dipole with a no-slip boundary, Comput. Fluids 35 (2006) 245–279.